SANDIA REPORT
SAND2011-8250
Unlimited Release
Printed October 2011

Progress toward Bridging from Atomistic to Continuum Modeling to Predict Nuclear Waste Glass Dissolution

Louise J. Criscenti, Peter A. Schultz, Carl Steefel, Peter Zapol, Ian Bourg

Prepared by
Sandia National Laboratories
Albuquerque, New Mexico 87185 and Livermore, California 94550

Sandia National Laboratories is a multi-program laboratory managed and operated by Sandia Corporation, a wholly owned subsidiary of Lockheed Martin Corporation, for the U.S. Department of Energy's National Nuclear Security Administration under contract DE-AC04-94AL85000.

Issued by Sandia National Laboratories, operated for the United States Department of Energy by Sandia Corporation.

Available to DOE and DOE contractors from
U.S. Department of Energy
Office of Scientific and Technical Information
P.O. Box 62
Oak Ridge, TN 37831

Telephone: (865) 576-8401
Facsimile: (865) 576-5728
E-Mail: reports@adonis.osti.gov
Online ordering: http://www.osti.gov/bridge

Available to the public from
U.S. Department of Commerce
National Technical Information Service
5285 Port Royal Rd.
Springfield, VA 22161

Telephone: (800) 553-6847
Facsimile: (703) 605-6900
E-Mail: orders@ntis.fedworld.gov
Online order: http://www.ntis.gov/help/ordermethods.asp?loc=7-4-0#online

SAND2011-8250
Unlimited Release
Printed October 2011

Progress toward Bridging from Atomistic to Continuum Modeling to Predict Nuclear Waste Glass Dissolution

Louise J. Criscenti
Peter A. Schultz
Geochemistry and Advanced Device Technologies Departments
Sandia National Laboratories
Albuquerque, New Mexico

Ian Bourg
Carl Steefel
Earth Sciences Division
Lawrence Berkeley National Laboratories
Berkeley, California 94701

Peter Zapol
Material Science Division
Argonne National Laboratory
Argonne, Illinois 60439

Abstract

This report summarizes research performed for the Nuclear Energy Advanced Modeling and Simulation (NEAMS) Subcontinuum and Upscaling Task. The work conducted focused on developing a roadmap to include molecular scale, mechanistic information in continuum-scale models of nuclear waste glass dissolution. This information is derived from molecular-scale modeling efforts that are validated through comparison with experimental data. In addition to developing a master plan to incorporate a subcontinuum mechanistic understanding of glass dissolution into continuum models, methods were developed to generate constitutive dissolution rate expressions from quantum calculations, force field models were selected to generate multicomponent glass structures and gel layers, classical molecular modeling was used to study diffusion through nanopores analogous to those in the interfacial gel layer, and a micro-continuum model (KμC) was developed to study coupled diffusion and reaction at the glass-gel-solution interface.

ACKNOWLEDGMENTS

The authors would like to acknowledge funding from the Department of Energy, Nuclear Energy Advanced Modeling and Simulation Integrated Performance and Safety Codes Program.

We would also like to acknowledge discussions with the International Corrosion Working Group members including Stéphane Gin, John Vienna, Joseph Ryan, Dennis Strachan, Carlo Pantano, Karl Mueller, and Jonathan Icenhower.

SANDIA National Laboratories is a multi-program laboratory managed and operated by Sandia Corporation, a wholly owned subsidiary of Lockheed Martin Corporation, for the U.S. Department of Energy's National Nuclear Security Administration under contract DE-AC04-94AL85000.

CONTENTS

FIGURES

TABLES

1 INTRODUCTION

1.1 Background

Borosilicate glass waste forms have been proposed to immobilize high-level nuclear wastes that result from reprocessing commercial spent nuclear fuel and nuclear weapons development (Grambow, 2006). Data collected to date suggest that glass waste forms offer the advantage that they can accommodate a wide range of waste streams, are resistant to radiation damage, and are relatively inert to both chemical and thermal perturbations. In order for these glass waste forms to be relied on in a geologic nuclear waste repository, however, their long-term durability must be established scientifically. Some of the scientific concerns for quantitatively assessing the performance of long-term disposal of nuclear waste materials involve reliably predicting interactions between the waste forms and the engineered and geologic systems over the long time periods for which the waste must be isolated from the biosphere. Half-lives of some radionuclides extend to millions of years, requiring isolation for geologic time periods. A key issue is to demonstrate that the waste forms will be durable for as long as 10,000 years, while the period of investigation that is possible in the field and the laboratory is relatively short.

The millennial-scale weathering rates of silicate glasses and minerals will play key roles in the fate of high-level nuclear waste in geological repositories (Ferrand et al., 2006; Frugier et al., 2008). Although these weathering rates cannot be probed directly, laboratory-scale weathering experiments (Ferrand et al., 2006; Icenhower et al., 2008; Cailleteau et al., 2011) and geochemical reconstructions (Maher et al., 2006) suggest that they are several orders of magnitude lower than the readily accessible short-term weathering rates of pristine silicate surfaces. Predictive models of these millennial-scale rates remain poorly constrained, and even the fundamental physical processes that cause their age-dependence have not been unambiguously identified (Casey, 2008; Frugier et al., 2008; Icenhower et al., 2008).

The rates of glass degradation observed from ancient glass artifacts are much slower than those observed in laboratory tests (Verney-Carron et al., 2010), similar to the slower degradation rates observed in nature for minerals (White and Brantley, 2003; Ganor et al., 2005; Hellmann and Tisserand, 2006; Bryan et al., 2009). Studies of natural and synthetic glass dissolution rates show far-from equilibrium behavior can be dependent on the Si (Wolf-Boenisch et al., 2004) and Al content (Hamilton et al., 2001) of the glass. The slower degradation rates observed in the natural systems may result from a number of differences between these systems and studies in the laboratory including dissolution mechanisms (Hamilton et al., 2001), glass reactive surface area (Wolf-Boenisch et al., 2004), and diffusion through intermediate phases (e.g., a gel layer; Cailleteau et al., 2008; Verney-Carron, 2010).

There are many different expressions that have been used to fit silicate dissolution data from leach tests in the laboratory. Many of these expressions rely on transition state theory (TST), where the activation energy associated with a complex mechanism defines the rate-limiting step in the dissolution process. Although TST is generally only considered appropriate for elementary reactions, it has been argued that if a complex mechanism is rate-limited by a single elementary reaction, then TST may be usefully applied to the overall reaction (Oelkers et al., 1994; Oelkers, 2001). Different dissolution behaviors, as defined by changes in solution

composition with time, are observed under far-from and near-equilibrium conditions. These different behaviors have often been fit with different rate expressions; partly because historically, the experimental data used to define the rate law did not extend over the entire range of geochemical conditions. For nuclear waste glass dissolution, these are the types of rate laws that have been implemented in the past. According to J. Vienna (*pers. comm.*), there are six different TST-based glass dissolution rate laws used in the nuclear waste glass community. This lack of consensus demonstrates we do not fully understand glass degradation processes and therefore cannot predict these processes over geologic time frames with confidence. Understanding long-term glass corrosion and developing models to predict this degradation with different glass compositions, waste streams, and environmental conditions is critical to the design of high-level waste forms and repository systems.

1.2 Nuclear Waste Glass Corrosion

Three distinct nuclear waste glass corrosion rate regimes are recognized (Van Iseghem et al, 2009) and illustrated in Figure 1-1:

I. An initial stage in which the rate of corrosion is relatively constant and at a maximum. This is also referred to as the forward (far-from equilibrium) rate of reaction, particularly in flow-through experiments where steady-state may be achieved. This stage occurs before the solution reaches saturation with respect to amorphous silica, at which point the corrosion has been observed to decrease markedly. It also occurs before any significant development of a leached layer can occur, although some workers (Frugier et al., 2008; Gin et al., 2011) have argued that a passivating layer limiting diffusive mass transfer can develop almost immediately.
II. A long-term corrosion rate regime that in experimental studies is observed to last as long as several years. The supposition in many of the analyses of geological waste repository performance is that this long-term rate regime may last for as long as the 10,000 years of the life history of the waste form. Existing studies have not yet unambiguously established whether this slowing of the rate is due to (a) saturation of the solution at the pristine glass surface (near-equilibrium) with respect to amorphous silica, or (b) the formation of a leached layer and a diffusion rate limitation. Unfortunately, in batch systems it is often very difficult to distinguish between diffusion-limited and near-equilibrium dissolution rates. In any case, it is essential that the mechanism for this slow rate regime be understood.
III. A late stage observed in only some experiments, in which the rate accelerates, apparently as the result of the formation of new crystalline phases (e.g., smectite, zeolites). As with Stage II described above, the same debate over chemical versus transport-dominated rates arise, with hypotheses that the increased rates could be due to either the local consumption of silica by mineral precipitation reactions or to an increase in the diffusivity of the reactive layer armoring the pristine glass.

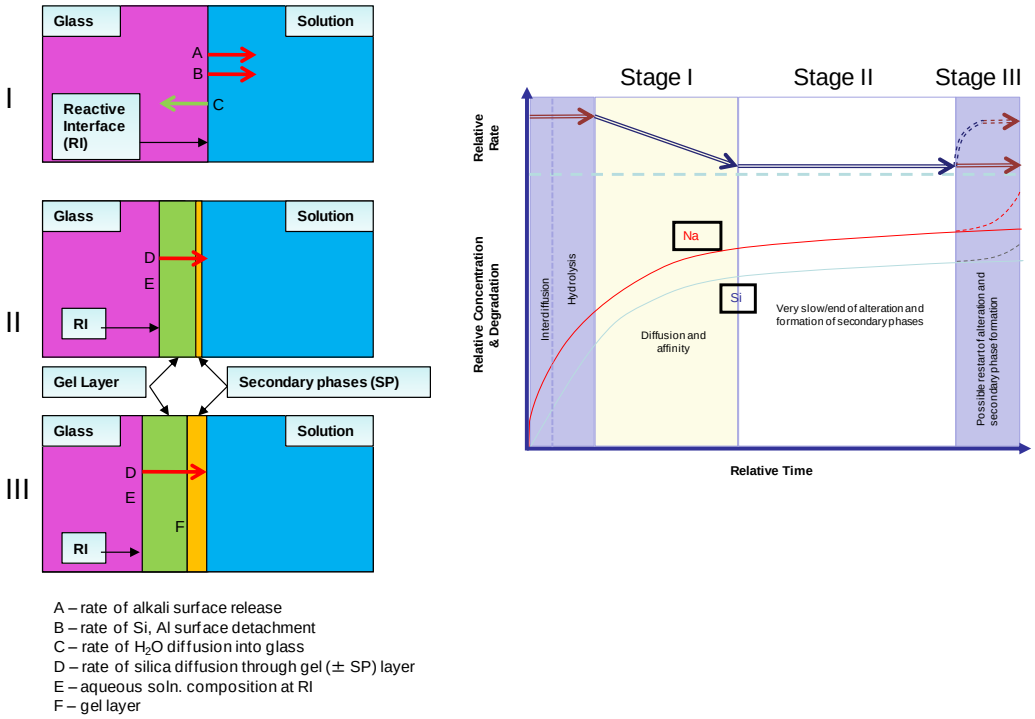

Figure 1-1. Anatomy of glass dissolution.

1.3 Objectives and Progress

The approach proposed by the Nuclear Energy Advanced Modeling and Simulation (NEAMS) program to investigate nuclear waste glass degradation is to first use atomistic-scale quantum and molecular modeling methods in combination with nanoscale experimental data to develop a complete mechanistic understanding of the processes involved in glass corrosion, and then incorporate information from the validated atomistic models into new constitutive equations and continuum-scale models to more effectively predict the chemical and physical changes observed at the continuum scale. Making the link between atomistic-scale, interfacial processes and constitutive equations that describe bulk continuum-scale observations has always been a challenge. However, both analytical and modeling approaches to investigating processes at the atomic scale have improved greatly in the last twenty years, and with the advent of more advanced computational capabilities, it now is possible to consider designing continuum-scale models from first principle calculations.

The objectives of the NEAMS subcontinuum task are (1) to demonstrate that atomistic modeling can provide an understanding of these mechanisms and their relative importance over time and in different physical and chemical environments, regardless of glass, waste, and solution compositions; and (2) to provide methods to incorporate the atomistic results into continuum-scale models. **An important accomplishment for this year has been the development of an integrated plan to tackle the unresolved questions regarding glass dissolution through modeling efforts from the atomistic to the continuum scale, supported at each scale by experimental validation.** Figure 1-2 and Figure 1-3 illustrate the overall modeling plan and the integrated approach developed between laboratories combining both computational and experimental strengths to bridge our understanding of glass degradation from the molecular to the continuum scale.

During the past year (October 2010 – September 2011), we have focused on developing methods to incorporate atomistic-scale, mechanistic models and data of the chemical and physical processes occurring in Regimes I and II of nuclear waste glass degradation into continuum-scale models. In parallel, a kinetic micro-continuum model (KμC) has been developed that can use different parameter sets (i.e., first-principle-derived parameters or semi-empirical parameters) to calculate all of the processes involved in Stages I – III of nuclear waste glass dissolution. The next three sections of this chapter summarize our approach to model development for the three regimes and plans for outlying years.

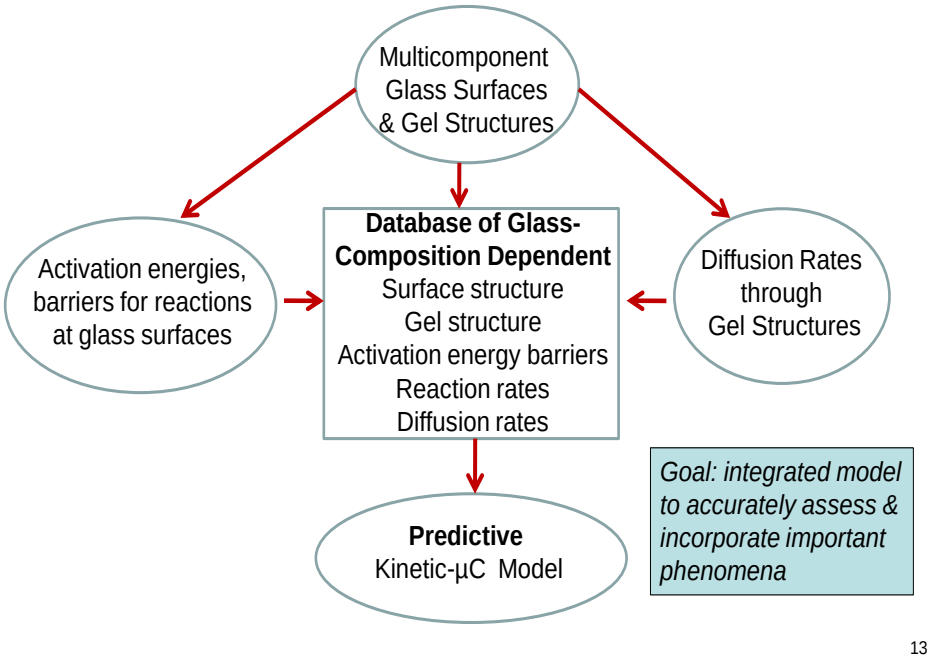

Figure 1-2. Modeling flow-chart illustrating atomistic-scale input into continuum-scale model.

1.3.1 Stage 1. Far-from Equilibrium Dissolution

It is generally assumed that the release of radionuclides from a nuclear waste glass will occur as a result of the breakdown of the glass framework consisting of network-forming cations (B, Si, and Al) bonded to oxygen atoms. This assumption underlies the design of simplistic nuclear waste glass degradation studies that emphasize understanding observed changes in aqueous silica as a function of time. A second mechanism for radionuclide release is through ion exchange within the glass itself. It has been proposed that ion exchange within the glass itself occurs independently and proceeds faster than the dissolution of the glass framework, and may be all that is required to release some radionuclides. To date, this hypothesis has not been substantially evaluated either through experiment or modeling in the nuclear waste glass community.

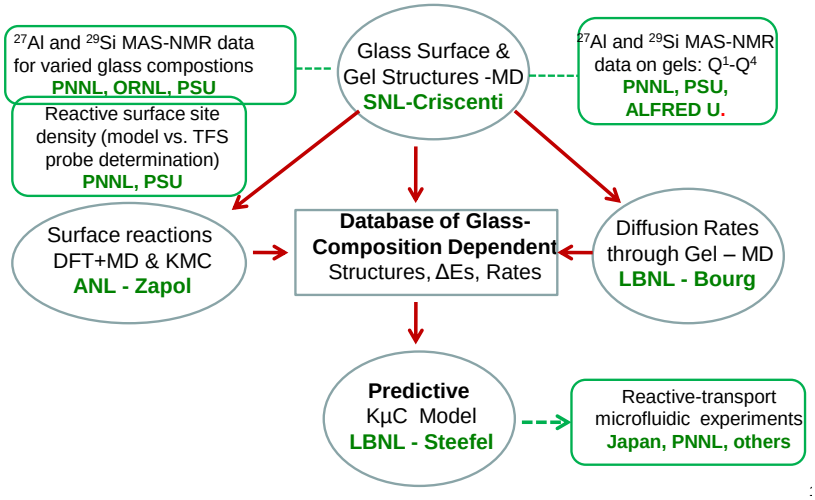

Figure 1-3. Flow chart illustrating coordinated modeling and experimental program effort.

During the past year, the NEAMS program in synergy with the NE FC R&D program have moved forward with the premise that the critical first rate-limiting step in nuclear waste glass degradation is the breaking of glass network bonds at the glass-water interface. Different cation-oxygen bonds have different strengths and associated activation energies, and these differences will impact the rate of release into solution for the different cations. Silica and boron, for example, may be released at different rates at low pH, as shown by Inagaki et al (2009). The hydrolysis of bridging T-O (T = Si, Al, B) bonds in a glass is often considered to be the rate-limiting step or steps in glass dissolution. In continuum experiments, the rate of hydrolysis appears to decrease in Regime II dissolution as silica concentration in solution rises (Grambow, 2006; Frizon et al, 2009), although it is still unclear whether the silica in solution slows the hydrolysis reactions, or simply results in preservation of silica in a gel layer that passivates the pristine glass surface. This "chemical affinity" effect has been described with Transition State Theory (TST) rate formulations similar to those used for mineral dissolution (e.g., Aagaard and Helgeson, 1982; Icenhower et al, 2008). The slowing of the rate as a result of silica saturation has been referred to as a "pseudo-equilibrium" state, because the solubility of the borosilicate glass cannot be rigorously defined in terms of the saturation with respect to a silica phase alone.

In Stage 1, the pristine glass surface is exposed to aqueous solution. Geochemists have made some progress in understanding the mechanisms of glass dissolution using quantum methods on small atomic clusters to calculate the energy required to break bonds on silicate mineral and glass surfaces. The atomic clusters are designed to represent a fragment of the glass network or mineral structure exposed to water. Activation energy barriers and reaction paths are calculated for H_2O, H_3O^+ or OH^- attack on T(Si, Al)-O bonds. However, comparisons between these calculated activation energy barriers and those determined from batch dissolution experiments are only useful if the overall dissolution of the solid is rate-limited by one type of reaction.

Orthoclase ($KAlSi_3O_8$) dissolution rates have been well studied, particularly under acidic conditions, both using flow-through reactors (Schweda, 1989) and by X-ray reflectivity experiments on two different crystal surfaces – the (001) surface and the (010) surface (Fenter et al., 2003). The X-ray reflectivity data for the dissolution of two orthoclase surfaces with

different surface site types and concentrations can be used to evaluate quantum-based predictions of mineral dissolution. Zapol's group at Argonne National Laboratory dedicated much of this year to using quantum methods to calculate the activation energies associated with breaking the different framework bonds exposed on the (001) and (010) surfaces through reactions with H_2O.

These activation energies were then incorporated into a Kinetic Monte Carlo (KMC) model to calculate the collective behavior of multiple, simultaneously-occurring reactions on each surface and then generate dissolution rates. These rates, calculated from first principles, over a range of pH values successfully match those experimentally determined by Fenter et al. (2003). Finally, a new constitutive equation for orthoclase dissolution was derived from the quantum-based activation energy barriers for bond-breaking and crystal structure data. The "upscaling" concept used is illustrated in Figure 1-4.

The next step toward successfully incorporating atomistic model-derived dissolution mechanisms into continuum-scale rate models for glass dissolution is to add incremental complexity to the system studied. The approach that will be taken in the next year is to move from a regular crystalline surface to the more random, complex structure of an amorphous glass. Starting with a simple three-component glass (e.g., Si-B-O or Si-Al-O), chemical complexity will be added until molecular models of 5-component glasses containing silicon, aluminum, boron, oxygen and sodium (Si-Al-B-O-Na) have been generated using classical molecular dynamics simulations. Preliminary research has been conducted at Sandia National Laboratories to select appropriate force field models to develop a self-consistent database of 3-, 4-, and 5-component glass compositions that will represent simplified nuclear waste glass compositions.

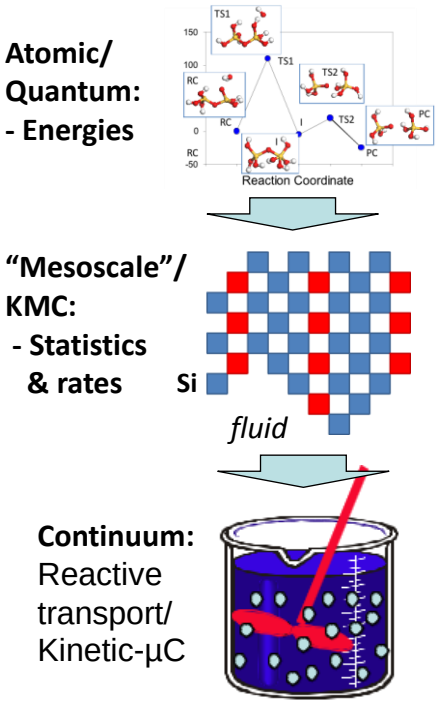

Figure 1-4. Schematic of "upscaling" from atomistic to continuum scale.

The availability of good nanoscale dissolution data for orthoclase was invaluable for developing and validating an upscaling methodology for orthoclase dissolution. Unfortunately, this type of data cannot be collected for glass dissolution because X-ray reflectivity is only useful for crystalline materials. However, information on bulk glass, glass surface, and glass gel structures is available from nuclear magnetic resonance (NMR) data (e.g., Pierce et al., 2010). Quantitative structural data about the local chemical environments of different glass species can be determined by NMR and used to define the extent of disorder in the tetrahedral network structure, the role of minor structural species such as Al cations with five instead of four oxygen neighbors, and the positions of non-bridging oxygens in certain glass compositions. Triple quantum magic angle spinning (3QMAS) NMR is used to count the fractions of non-bridging oxygens and various network linkages such as Si-O-Si, Si-O-Al, and Al-O-Al. In addition, this technique can be used to determine the ratio of three-fold- and four-fold-boron within a glass structure. NMR is essentially the only known way of quantifying these details in a glass, and these details are critical to validating molecular models of glass structure. Simulated multicomponent glass and glass surface structures will be validated against published NMR data or data collected by Mueller's group at Pacific Northwest National Laboratory.

1.3.2 Stage 2. Near-Equilibrium Dissolution

Stage 2 glass degradation is defined as occurring after the formation of a gel at the glass surface. There are now two interfaces to be considered - the glass-gel interface and the gel-water interface - as well as the porous gel in between. The porous gel may be further subdivided to include a passive reactive interface (PRI) defined by Frugier et al. (2009). Chemical reactions may occur at the glass surface, within the gel structure, or at the gel-aqueous solution interface. In addition, diffusion through the gel of glass components into the solution and aqueous species to the glass surface occurs. Transport by diffusion through the gel layer may limit overall glass dissolution rates. The thickness of the gel layer varies over time and is also dependent on glass composition. Frizon et al. (2009) argue that as the rate of hydrolysis at the glass surface diminishes the thickness of the gel layer increases. This could be a result of high silica concentration in solution which will favor the precipitation or preservation of a gel layer. At low silica concentrations, the gel layer dissolves in addition to the pristine borosilicate glass.

The recondensation and densification of the silica-rich gel layer is described by Cailleteau et al (2008). They demonstrated that by including zirconium up to 8% in the glass mixture, it was possible to suppress this recrystallization and densification reaction, suggesting that the zirconium has the effect of preserving part of the residual glass structure. In the absence of zirconium, however, the silica gel is observed to densify, as supported by both TEM and SAXS measurements. As a result, the effective diffusivity in the gel decreases substantially to the point where a diffusion barrier develops that limits the rate of corrosion to a low value.

Over the past year, the main thrust of our modeling effort toward understanding the contribution of the gel to glass dissolution rates has been to use classical molecular dynamics to understand the diffusion of water through silica nanopores. This work has been conducted at Lawrence Berkeley National Laboratory by Bourg. Idealized silica gel layer nanopores (cylindrical pores with 6 nm length and 1 or 2 nm diameter) have been performed in order to determine how strongly the properties of nanoconfined water differ from those of bulk liquid water. For 1-nm-diameter pores and 2-nm-diameter pores, water diffusion coefficients of 0.27 ± 0.08 and $1.06 \pm$

0.16×10^{-9} m^2 s^{-1} are determined respectively. These diffusion coefficients are smaller than the self-diffusion coefficient of bulk liquid water at 298 K, suggesting that water diffusion through the silica gel layer will be slower than in bulk solution. In addition, these calculations suggest that silica surface sites on curved nanopore walls such as those present in the gel structure, may be less acidic than those on flat silica surfaces.

Concurrently, colleagues at Pennsylvania State University (Pantano, Mellott, and Leed) have used a suite of analytical techniques and classical molecular dynamics simulations to study the formation of gel layers on glass surfaces. Mellott (2003) found through experimental analysis that surface layers on Ca-Na-Al-Si-O glasses were microporous, more structurally ordered than glass, and contained primarily 3-membered and 4-membered rings. This local transformation after partial dissolution left the micromorphology features (SEM-scale) intact but changed the nanotopography (AFM-scale). To determine if the gel structure could be derived from the condensation of a leached layer consisting only of silica, Mellott (2003) performed preliminary molecular dynamics calculations to investigate how a leached layer might condense to form a gel-like structure. The calculated ratio of Q species (i.e., Q^1, Q^2, Q^3, and Q^4) in the condensed layer closely matched ^{29}Si MAS-NMR data, suggesting that condensation may play a key role in gel formation. In addition, both the MD simulations and ^{29}Si MAS-NMR data suggested that an increase in concentration of Na_2O in the bulk glass composition results in an increase in the degree of polymerization of the surface layer.

Multinuclear solid-state NMR investigations of the structure of the amorphous gel layers that form during the aqueous alteration of silicate glasses have also been conducted in the nuclear waste glass community (e.g., Frederic et al., 2006). The glass compositions studied were of increasing complexity, with addition of aluminum, calcium, and zirconium to a sodium borosilicate glass. Two series of gels were obtained, in acidic and in basic solutions, and were analyzed using ^{1}H, ^{29}Si, and ^{27}Al MAS NMR spectroscopy. Advanced NMR techniques were employed such as ^{1}H-^{29}Si and ^{1}H-^{27}Al cross-polarization (CP) MAS NMR, ^{1}H double quantum (DQ) MAS NMR and ^{27}Al multiple quantum (MQ) MAS NMR. Under acidic conditions, ^{29}Si CP MAS NMR data show that the repolymerized silicate networks have similar configurations. The gel porosity is influenced by the pristine glass composition, modifying the silicon-proton interactions. From ^{1}H DQ and ^{1}H-^{29}Si CP MAS NMR experiments, it was possible to discriminate between silanol groups (isolated or not) and physisorbed molecular water near Si(Q^2), Si(Q^3), and Si(Q^4) sites, as well as to gain insight into the hydrogen-bonding interaction and the mobility of the proton species. Alteration in basic media resulted in a gel structure that is more dependent on the initial glass composition. The availability of these new structural data should provide a better understanding of the impact of glass composition on the gel structure depending on the nature of the alteration solution.

It is part of our integrated research plan to generate glass gel layers using a classical molecular dynamics approach analogous to Mellott (2003) for different multicomponent glass compositions and characterize the gel structures created for these compositions. The gel structures generated will be derived from the simulated and validated glass structures discussed in Section 1.3.1. They will be validated with reported NMR data in the literature on gels or through additional NMR studies performed Mueller at PNNL. These simulated structures will then be used to calculate apparent diffusion constants for water and ions through the gel layer under different conditions.

1.3.3 Comprehensive Continuum-Scale Model

In addition to starting from the atomistic scale on simplistic systems, a kinetic micro-continuum model (KμC) that incorporates both reaction and transport processes was developed this year by Steefel at LNBL. At present, this model is populated with rate laws and parameter sets that are not based on a full mechanistic understanding of glass dissolution. Ultimately, we seek to incorporate both chemical species-specific diffusion coefficients for transport through the gel layer and activation energies for glass dissolution derived from molecular models into the KμC model. In the meantime, expressions derived from macroscopic experiments have been incorporated into the coupled model to account for (1) diffusion of H_2O through the pristine glass and its alteration products, (2) multicomponent diffusion of ions through the glass corrosion products, (3) ion exchange between water and the cations in the glass, (4) kinetically controlled hydrolysis reactions resulting in breaking of glass network bonds (Si, B, Al), (5) precipitation reactions for amorphous and/or crystalline phases of variable composition that are kinetically and thermodynamically controlled, (6) kinetically controlled ripening and/or densification reactions that can reduce the diffusivity of the corrosion products, (7) kinetically and thermodynamically controlled formation of new crystalline phases (e.g., smectite, zeolite), with possible consequences for the transport properties of the corrosion layer, and (8) flow and diffusion in the aqueous phase adjacent to the glass surface. These processes and parameters are tunable so that they can capture different corrosion behavior under different conditions.

At present, this is the only model developed that can account for the rapid increase in silica concentration in solution that occurs in Stage III, if in fact, this increase is due to the precipitation of one or more crystalline phases in the gel layer. Zeolites have been reported in alkaline solutions, and the formation of these phases often leads to the resumption of a relatively high rate of borosilicate glass corrosion. Whether this increase in corrosion rate is due to the local suppression of silica concentration at the pristine glass surface or it reflects the breakdown of a dense PRI structure that limited diffusive transfer remains unclear.

2 DEVELOPMENT OF FIRST PRINCIPLES-BASED MODELS FOR GLASS DISSOLUTION

2.1 Background

Recently, evidence has emerged to indicate that the most fruitful path to achieving understanding of dissolution processes is likely to be through modeling and experiments designed to study the surface processes at the molecular level. To make use of subcontinuum modeling, approaches are needed for assessment and development of constitutive models than can predict the dissolution kinetics of glass exposed to aqueous solution environments. It is recognized that investigation of surface processes involved in the dissolution rate of glass is particularly difficult because of the lack of long-range order in the surface structure and because the surfaces may reorganize extensively as they interact with water during the dissolution process (Lasaga, 1998; Verney-Carron et al., 2010). Because similar processes have been observed to control the dissolution rates of silicate minerals and silicate glasses (Verney-Carron et al., 2010; Casey et al., 1993), studies of the dissolution of crystalline silicates can be used initially to provide important insights into the molecular-level mechanisms of glass dissolution. *The overall task is to establish a first-principle-based predictive model for the dissolution kinetics of different compositions of glass waste forms exposed to aqueous solutions*.

A typical approach to a constitutive model is based on a postulation, often implicit, of chemical processes at the interface and assigning effective activation energies and proton activities that are determined by fitting the resulting equation to experimental data. For example, while the expression

$$R = k_0 10^{-\eta pH} exp\left[\frac{-E_a}{RT}\left(1 - \frac{Q}{K_{eq}}\right)\right] + r_\infty \quad (2.1)$$

works well in many cases, it lacks a mechanistic basis for systematic improvement. It has been recognized for a long time that quantum chemistry can be extremely useful in determining rate-limiting steps and evaluating reaction pathways in silicate minerals and glasses (Lasaga, 1998; Verney-Carron et al., 2010; Gibbs, 1982; Pelmenschikov et al., 2000). To improve the model systematically, the rates of elementary reaction steps and the reaction site concentrations must be determined and introduced into a kinetic equation or a kinetic numerical model. Kinetic models based on experimental observations have been developed previously (Oelkers, 2001). However, it is more accurate to perform a Kinetic Monte Carlo (KMC) simulation based on first-principles results (Nangia and Garrison, 2009a; Zhang and Luttge, 2009). This modeling removes assumptions regarding the mechanism and functional form for the dissolution rate.

During the past year, molecular-level model development has been based on using the dissolution of crystalline orthoclase ($KAlSi_3O_8$) as a proxy for glass. Orthoclase has a well-defined crystalline structure and there are many experimentally determined dissolution rates as a function of external conditions reported in the literature (see Figure 2-1). Orthoclase was selected for model development because X-ray reflectivity data is available on the dissolution of the (001) and (010) orthoclase surfaces (Fenter et al., 2003). The experiments show that the two surfaces have different dissolution rates that exhibit both temperature and pH dependences. In

addition the formation of both a gel layer and secondary phases on the orthoclase surfaces has been observed. Akin to glass surfaces, each orthoclase surface has several types of exposed surface oxygen atoms that differ in their protonation state (e.g., $SiOH_2^+$, SiOH, and SiO^-), the number of bonds they form with the crystalline matrix (Q^1, Q^2, Q^3, Q^4), and their connectivity to Al and Si in the matrix. In addition, the bulk and surface structures of both orthoclase surfaces are well reproduced by density functional theory (DFT) calculations. The major difference between orthoclase and a glass of the same stoichiometry is the well-ordered, crystalline nature of the mineral.

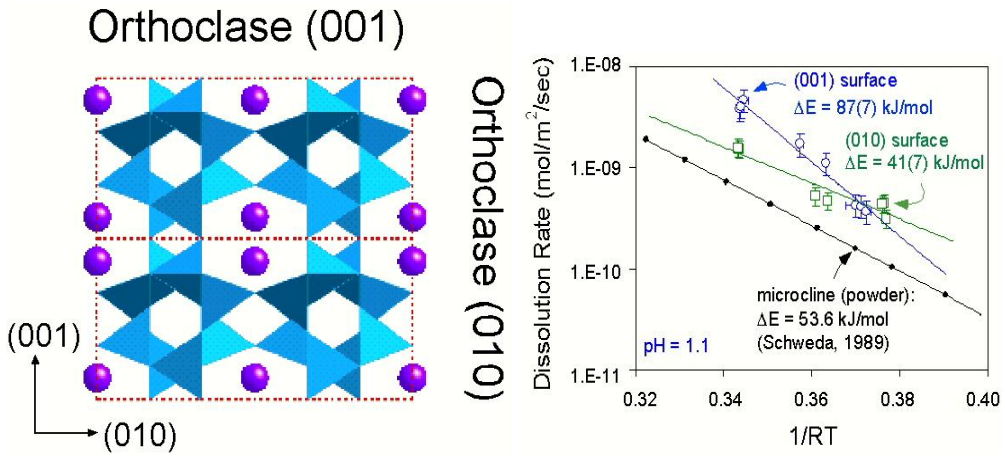

Figure 2-1. **Orthoclase structure and dissolution rate.**

2.2 Approach

The hydrolysis reaction barrier is found to depend on both the network connectivity and the protonation state. The apparent activation energy barrier for each surface can be calculated at different pH values by taking into account the distribution of surface sites at a given pH and the activation energies for all sites on the surface. This barrier will be a function of the activation energy barriers for breaking each bond at the orthoclase surface. Using density functional theory (DFT), the activation energy barriers for breaking each (Si, Al)-O bond at the surface are calculated using a periodic slab model. Initially, each orthoclase surface is characterized by one or more of the following: non-bridging oxygen atoms and bridging oxygen atoms bonded to Q^3(Si, Al) and/or Q^4(Si, Al), where, for example, a Q^3(Si, Al) is bonded to three oxygen atoms within the orthoclase structure. Upon breaking one T-O bond, where T = Si or Al, a Q^m(T) will progressively become a Q^{m-1}(T), Q^{m-2}(T) site until it becomes a solution species (Q^0). Each surface site will undergo the same types of transformations during dissolution. The overall rate, *k* is a linear combination of rates for all exposed sites.

The charge on each surface site, *i*, is a function of the pH of the solution. In addition to the connectivity of each surface site to the bulk crystal structure, the charge of the surface site will impact the hydrolysis reaction mechanism and corresponding activation energy barrier associated with hydrolysis. Therefore, the final rate expression generated from atomistic calculations must include information regarding the connectivity of the surface sites and their protonation at a specific pH. The expression used is:

$$k = \sum_{structure(Q)} \quad \sum_{protonation(i)} n_Q f_{Qi} k_{Qi} \tag{2.2}$$

where

$$f_{Qi} = f(Q, i, aq, pH) \tag{2.3}$$

and

$$k_{Qi} = A_{Qi} e^{-E_a(Q,i)/RT} \tag{2.4}$$

The major model components to be determined are E_a and f_{Qi}, where E_a is the activation energy for bond breaking, and f_{Qi} is the fraction of surface site type (Q, i). The fractional distribution of positive, negative, and neutral sites for each Q varies with pH. Each site type (Q^4, Q^3, Q^2) has a different rate constant k_{Qi} that is a function of pH.

Figure 2-2 illustrates the mechanisms for hydrolysis for protonated, neutral, and negatively charged surface sites and Figure 2-3 illustrates the activation energy barriers calculated using DFT-PBC (where PBC is short for periodic boundary conditions) for breaking each possible T-O bond on the orthoclase surfaces as a function of connectivity and pH. Using DFT, the activation energy barriers for breaking each (Si,Al)-O bond of the surface bridges [(Si,Al)-O-(Si,Al)] have been calculated using a periodic slab model. The calculated E_a varies with both Q^m and Q^n for T^m-O-T^n in a non-monotonic way. The calculated activation energy is significantly lower for protonated ($SiOH_2^+$) or deprotonated (SiO^-) surface sites than for neutral sites. The breaking of an Si-O bond in an Si-O-Al bridge also, generally has a lower E_a than an Si-O-Si bond. These results are consistent with other quantum-based calculations that have been reported in the literature (Nangia et al., 2009b; Morrow et al., 2009; Nangia et al., 2008; Criscenti et al. 2006; Laurence et al., 2003; Pelmenschikov et al. 2000; Lasaga 1994, 1996).

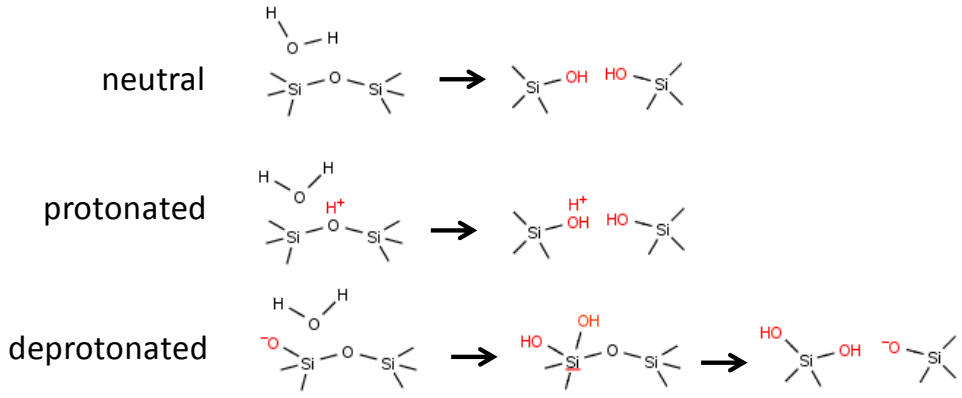

Figure 2-2. Hydrolysis reactions of Si-O-Si under different protonation states.

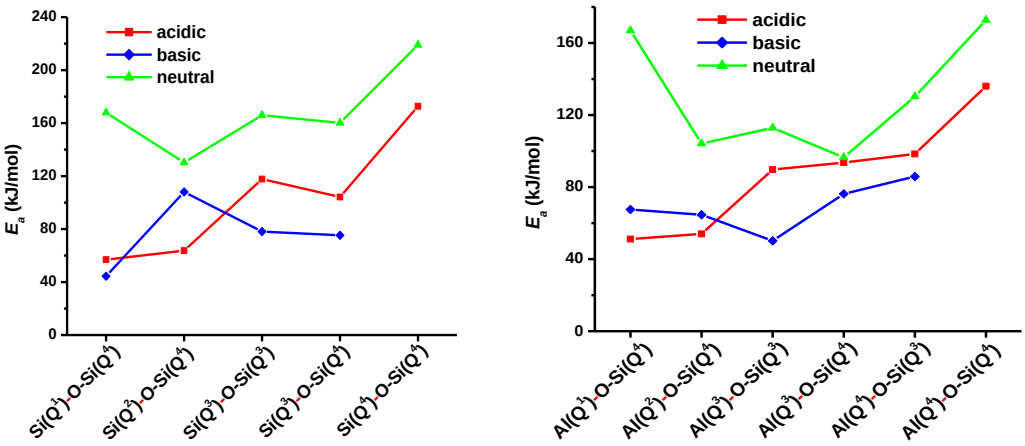

Figure 2-3. Activation energies for orthoclase surface sites.

In order to calculate the specific H coverage on each surface as a function of pH, numerous states *j*, each having a specific H coverage and a certain distribution of three sites $SiOH_2^+$, SiOH, SiO^- (c_{ij}) were generated. The change in free energy for each state ΔG_j (also a function of pH) was calculated according to:

$$\Delta G_j = \Delta E_j(nH^+_{SURF}) - n_j\mu(H^+, aq, pH) \tag{2.5}$$

$$\mu(H^+, aq, pH) = \mu_0(H^+) - 2.303kT \cdot pH \tag{2.6}$$

The probability for each state at a given pH is given by a Boltzmann distribution:

$$\rho_j = \frac{e^{-\Delta G_j/k_BT}}{\sum_k e^{-\Delta G_j/k_BT}} \tag{2.7}$$

The actual fractional number (normalized) of site *i* is:

$$f_i = \sum_j c_{ij}\rho_j \tag{2.8}$$

The calculated distribution of protonated, neutral, and deprotonated sites as a function of pH provides a calculated point of zero net proton charge (PZNPC) that agrees with the feldspar experimental data available (3.0 – 6.1; Stillings et al., 1995). The protonation scheme varies with different surface orientations and compositions. For a Si-rich (001) surface the calculated PZNPC is 3.5, for the stoichiometric (001) surface, the PZNPC is 4.5, and for an Al-rich (010) surface, the PZNPC is 6.4. These results are consistent with the fact that silica has a low PZNC (~ 2.0) and Al-oxide minerals have a PZNPC between 7 and 8.

Model predictions versus orthoclase dissolution data as a function of temperature and pH are illustrated in Figure 2-4. The first fit to the data is consistent with DFT-calculated activation energy barriers for Q^3Si and Q^3Al to calculate an overall apparent activation energy barrier. The second fit represents orthoclase dissolution curves consistent with calculated activation energy

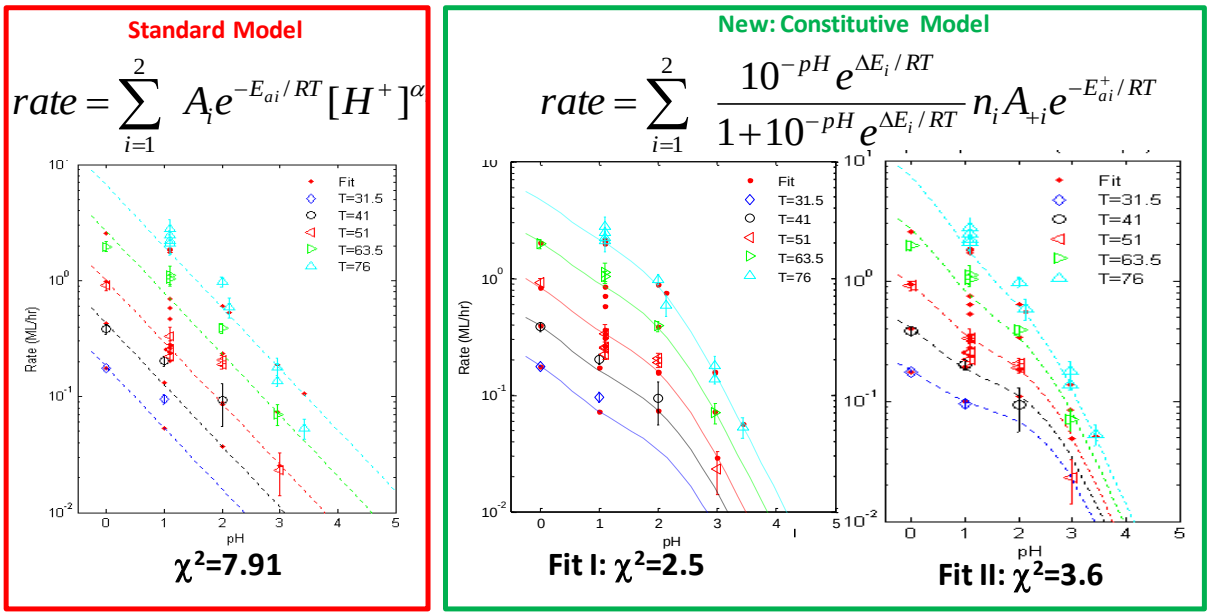

Figure 2-4. Validation of first-principles-based constitutive models.

barriers for Q^1Si, Q^2Si, and Q^3Si.

Using the KMC approach with reaction barriers and site distributions from first principles calculations, dissolution rates for the (001) and (010) surfaces at 350K were calculated at pH 1.1

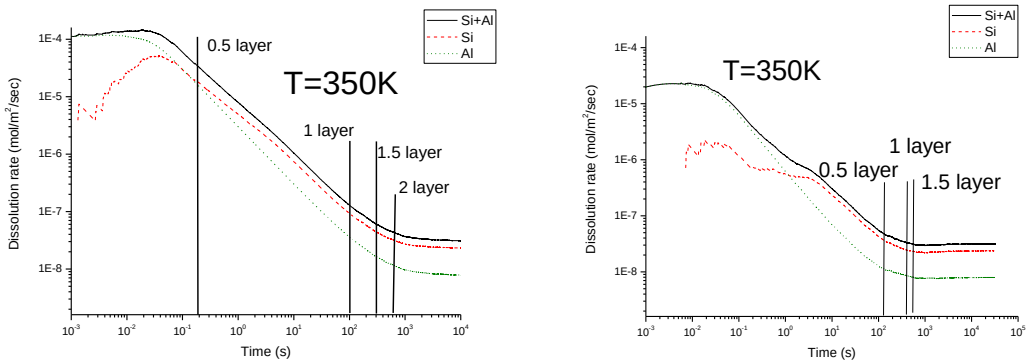

Figure 2-5. Simulated dissolution of orthoclase as a function of Si and Al removal from the surface. The (001) surface is illustrated on the left; the (010) surface on the right.

(see Figure 2-5). Preliminary results indicate that dissolution is congruent. The dissolution rate reaches a steady state value after several monolayers and surface roughness increases with time. Initially (001) dissolves faster than (010) which is in good agreement with experiment.

In summary, a new constitutive model for the initial, far-from-equilibrium dissolution rate of crystalline aluminosilicates has been developed based on (1) elementary steps of hydrolysis reactions for Si(Q_m)-O-T(Q_n) (T=Si, Al) and (2) protonated/deprotonated surface site distributions. The model fits well with experimental data. Both (1) and (2) were determined for orthoclase using first-principles quantum calculations. Kinetic Monte Carlo is used to simulate dissolution and test the predictions of the new constitutive model.

3 MOLECULAR DYNAMICS SIMULATIONS OF WATER CONFINED IN SILICA NANOPORES

3.1 Introduction

To begin addressing the influence of the silica gel layers that develop at the glass-water interface during dissolution and appear to control long-term glass dissolution rates (Stage II), molecular dynamics (MD) simulations of water in idealized silica gel layer nanopores (cylindrical pores with 6 nm length and 1 or 2 nm diameter) have been performed in order to determine how strongly the properties of nanoconfined water differ from those of bulk liquid water. Because of the nanoporous nature of gel layers, the properties of silica-water interactions are likely to be different than for silica in bulk water. The nanoporous nature of the gel layer may result in different water diffusion coefficients as well as in different interfacial reactions (e.g., proton exchange between water and the silica surfaces) than in bulk water.

Two key properties of water in silica gel layers that may be modulated by nano-confinement are, its diffusion coefficient and its acid-base reactivity with silica surfaces. The first effect is well established in nanoporous media (Bourg and Sposito, 2010) but it has never been quantified in nanoporous silica gels. Existing models of silicate dissolution strongly differ by assuming that diffusion in silica gel layers is either fast (Oelkers, 2001) or rate-limiting (Frugier et al., 2008). Experiments have shown that diffusion is slow in at least some silica gel layers (Cailleteau et al., 2011), but they did not quantify the diffusion coefficient. The second effect is even more scarcely examined: only a few studies of nanoporous alumina (Wang et al., 2003), and imogolite mineral surfaces (Fernández-Martínez, 2009) have suggested that either nano-confinement or surface curvature can influence the pK_a values of surface functional groups. In the case of silica, the intrinsic pK_a value of silanol sites on flat surfaces is well established [$pK_{a,int}$ = 6.4 to 6.7 for the reaction $>SiOH \Leftrightarrow >SiO^- + H^+$ (Sonnefeld et al., 2001; Dove and Kraven, 2005)], but the influence of nano-confinement on this pK_a value (and hence on surface charge density in silica gel layers) is entirely unknown.

Molecular dynamics (MD) simulations are well suited for probing the structure and dynamics of water in nanopores (Rotenberg et al., 2007; Kerisit and Liu, 2009; Bourg and Sposito, 2010). They also have been used successfully to inform bond-valence models of the intrinsic pK_a values of surface functional groups at mineral-water interfaces (Machesky et al., 2007). To our knowledge, however, relatively few MD or Monte Carlo (MC) simulation studies have investigated water in SiO_2 nanopores (Joseph and Aluru, 2006; Leung et al., 2006; Cruz-Chu et al., 2006, 2009; Castrillón et al., 2009), and only one study used an amorphous SiO_2 structure and surface silanol groups at the solid-water interface (Leung et al., 2006). Leung et al. (2006) used grand canonical Monte Carlo (GCMC) and *ab initio* molecular dynamics (AIMD) simulation techniques to probe a ~1 nm diameter cylindrical nanopore in a small block of SiO_2 glass with >SiOH groups at the glass-water interface (< 400 atoms per simulation cell). They found that their pore structure was stable (i.e., >SiOH groups did not exchange protons with nanopore water) during 4.5 ps AIMD simulations. They also observed that their uncharged SiO_2 nanopore strongly attracted Na^+ and repelled Cl^- ions, thus confirming that the aqueous geochemistry of SiO_2 nanopores differs significantly from that of bulk liquid. We built upon the research of Leung et al. (2006) by simulating much larger systems (6-nm-long SiO_2 nanopores in

contact with two bulk water reservoirs; 16,794 atoms per simulation cell) for much longer durations (12 to 16 ns). We determined for the first time the diffusion coefficient of water in hydroxylated cylindrical silica nanopores and the influence of nano-confinement on the acid-base reactivity of surface sites for two pore diameters (1 and 2 nm) relevant to silica gels and other systems such as Vycor glass (Ricci et al., 2000).

3.2 Simulation methodology

Molecular dynamics simulations of SiO_2-water systems are sensitive to the choice of interatomic potential models, the main input to these simulations (Cruz-Chu et al., 2006; Joseph and Aluru, 2006; Skelton et al., 2011). Therefore, as a prelude to simulating water-filled SiO_2 nanopores, we tested a selection of SiO_2-water interatomic potential models against experimental data on the structure of SiO_2 glass (Ohno et al., 2001) and the density profile of water on the fully hydroxylated and protonated $(10\bar{1}0)$ surface of α-quartz (Schlegel et al., 2002). On the basis of test simulations, we adopted the CLAYFF model of Cygan et al. (2004). Then, we carried out MD simulations of water in cylindrical SiO_2 nanopores. Briefly, our simulated systems consisted of two 4.5-nm-thick water films located on either side of a 6-nm-thick infinite slab of SiO_2 glass and connected by a water-filled straight cylindrical nanopore with a diameter of 1 or 2 nm (Figure 3-1). Our systems (> 16,000 atoms in a 31.65 × 36.54 × 190.0 Å periodically-replicated simulation cell) were simulated for 16 or 12 ns (for 1- and 2-nm-diameter pores, respectively), after 3 ns of equilibration at 298 K. For all SiO_2 nanopore simulations, we used the extended simple point charge (SPC/E) water model (Berendsen et al., 1987), known to accurately predict the structure (Hura et al., 2003), diffusion coefficient (Smith and Dang, 1994), and static dielectric constant (Wasserman et al., 1995) of ambient liquid water, and the CLAYFF model (Cygan et al., 2004) for silica atoms. Unless otherwise specified, simulations were carried out in the *NVT* ensemble with a 0.5 fs time step; long-range (> 15.0 Å) Coulomb and van der Waals interactions were treated by Ewald summation with 99.99% accuracy. Temperature was controlled by coupling our simulated system to a Nose-Hoover thermostat with a coupling constant of 100 ps. All simulations were carried out with the code LAMMPS (Plimpton, 1995) and analyzed using in-house Matlab routines and the molecular visualization code VMD (Humphrey et al., 1996).

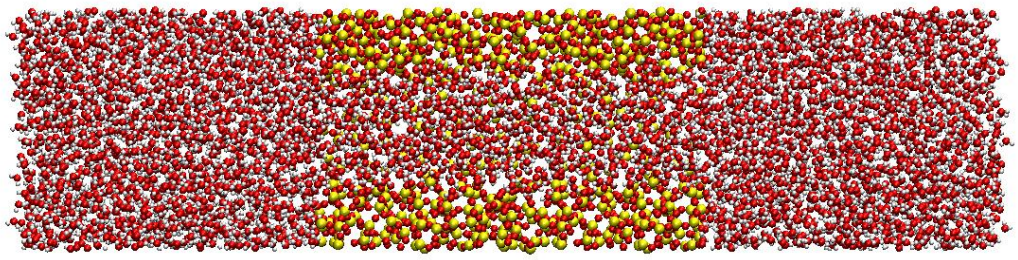

Figure 3-1. MD Simulation snapshot of 2-nm-diameter pore.
The pore is viewed along the *zy* coordinate and shows two 4.5-nm-thick water films (on the left and right sides) separated by a 6-nm-thick porous SiO_2 slab. The SiO_2 slab is drawn in cross-section to reveal the inside of the 2-nm-diameter cylindrical pore. The simulated system is 31.65 × 36.54 × 190.0 Å and includes a 4-nm-thick vapor gap between periodic images in the *z* direction.

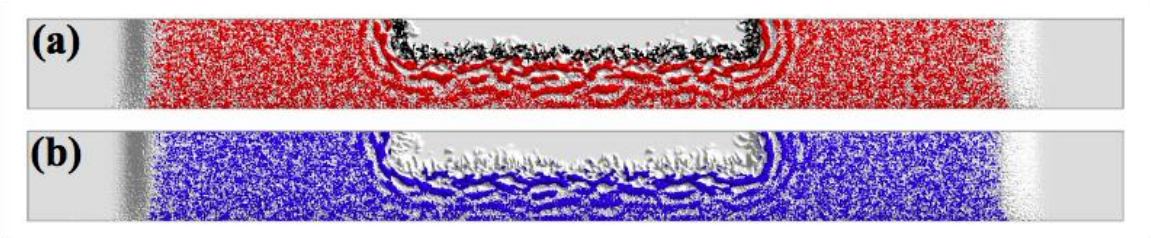

Figure 3-2. Density of water relative to bulk water.
(a) Average density of water O atoms (O_w, in red) and silica H atoms (in black) in the 2-nm-diameter pore simulation, plotted as a function of *z* (horizontal axis) and distance *r* from the pore axis (vertical axis). (b) Average density of water H atoms (H_w, in blue) in the same system. Red and blue colors indicate O_w and H_w densities greater than their average densities in the bulk liquid; black color indicates silica H atom densities greater than 10 mol dm^{-3}.

3.3 Simulation results

3.3.1 Interfacial water structure

Maps of the density distributions of water O and H atom (ρ_{Ow}, ρ_{Hw}) in our simulated systems (Figure 3-2) show that water is significantly structured by the silica surface. If we identify the location of the silica surface with the Gibbs surface of water obtained from $\rho_{Ow}(z,r)$ in Figure 3-2, the surfaces of the SiO_2 slab are located at $z = 64.3 \pm 0.1$ and 125.7 ± 0.1 Å (pore length 61.4 Å) and simulated pore radii are $r = 4.39$ and 9.37 Å. Plots of ρ_{Ow} and ρ_{Hw} vs. distance *d* (measured from Gibbs surface of water O atoms towards the aqueous phase) show density layering up to about three statistical water monolayers (~ 9 Å) from the silica surface (Figure 3-3), consistent with the behavior of water on a range of solid surfaces (Toney et al., 1995; Schlegel et al., 2002; Bourg and Sposito, 2011). Average water O and H density distributions on the flat external surfaces and concave pore walls of our simulated silica structures (Figure 3-3a, b) are essentially identical beyond the first statistical water monolayer ($d > \sim 3$ Å). However, in the first statistical water monolayer, water H atom density differs significantly between flat and curved surfaces (Figure 3-3c): ρ_{Hw} on flat external surfaces has a peak at $d = 1.0 \pm 0.1$ Å (in addition to its main peak at $d = 2.3 \pm 0.2$ Å) that is absent for ρ_{Hw} on the curved nanopore walls. This peak results from H-bonds donated by water molecules to surface O atoms, and its absence in cylindrical silica nanopores indicates that H-bond donation from water to surface O atoms is weaker in these nanopores than on flat silica surfaces. To our knowledge, this is the first time that the molecular-scale interactions of water with a pore surface that is concave towards the water phase are shown to differ from their interactions with an otherwise isostructural flat surface.

3.3.2 Water diffusion through silica nanopores.

Water diffusion through cylindrical silica pores was probed by "tagging" all water O atoms according to the bulk water reservoir in which they were last located. Water molecules initially located inside the pore ($64.3 < z < 125.7$ Å) were left untagged until they entered one of the bulk water reservoirs. Calculated density distribution profiles of tagged O atoms (plotted for several time intervals after the beginning of the MD simulations) and the cumulative "breakthrough

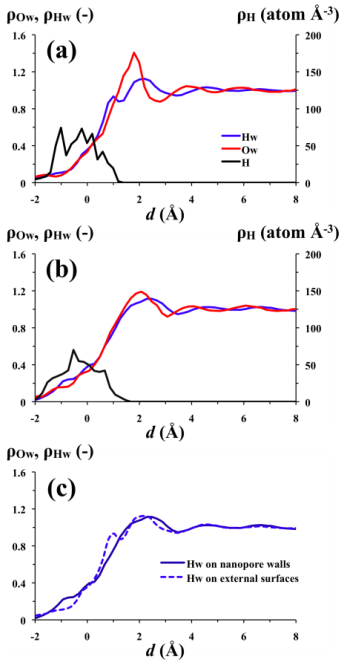

Figure 3-3. Average density of atoms as a function of distance from pore surface. (a) Average density of silica H (black), O_w (red), and H_w atoms (blue) in the 2-nm-diameter pore simulation as a function of distance from the surface, calculated for a 367 Å^2 region of the flat external surface (r = 13.6 to 15.6 Å). (b) Same as Figure 3-3a for a 353 Å^2 region of the curved nanopore surface (z = 92 to 98 Å). (c) Comparison of H_w density profiles on flat and curved surfaces.

flux" of water O atoms are shown in Figure 3-4 for the 2-nm-diameter pore simulation. Our simulations show, firstly, that durations greater than about 8 ns are required to probe steady-state water diffusion ((characterized by a time-invariant curve in Figure 3-4a and a time-invariant slope in Figure 3-4b) through 6-nm-long silica pores. Secondly, the linearity of calculated steady-state concentration profiles (Figure 3-4a) indicates that the local diffusion coefficient of water is invariant with z; in particular, this means that water molecules exchange freely between the nanopore and the bulk liquid reservoir, in contradiction with the extant Renkin-Pappenheimer model of diffusion in nanopores (Renkin, 1954; Prakash et al., 2008). Finally, the steady-state fluxes determined here (during t = 8 to 16 ns for the 1-nm-diameter pore and t = 9 to 12 ns for the 2-nm-diameter pore) yield water diffusion coefficients of 0.27 ± 0.08 and $1.06 \pm 0.16 \times 10^{-9}$ m^2 s^{-1} in the 1 and 2 nm-diameter-pores, respectively.

When normalized to the self-diffusion coefficient of bulk liquid water [$D_0 = 2.299 \times 10^{-9}$ m^2 s^{-1} at 298 K (Mills, 1973)], our simulation results yield a "constrictivity factor" $\delta = D_{nanopore}/D_0$ of 0.12 ± 0.03 or 0.46 ± 0.07 in the 1- and 2-nm-diameter silica pores, respectively. Interestingly, these values are close to the fraction of water molecules in each pore that is not located in direct contact with the surface {0.10 and 0.46, respectively, calculated as $[(r_{pore} - h_{water})/r_{pore}]^2$, where r_{pore} (Å) is the pore radius and h_{water} = 3 Å is the thickness of a statistical water monolayer}. The slow diffusion of water in silica nanopores is in line with results reported for other hydrophilic nanoporous media (Kerisit and Liu, 2009; Bourg and Sposito, 2010). [Conversely, in

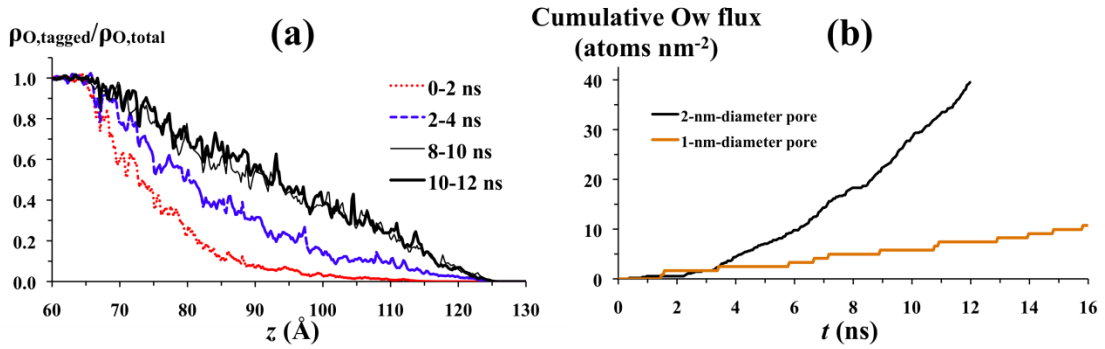

Figure 3-4. Density distribution of water molecules that have diffused through the pore. (a) Density distribution of "tagged" O atoms (normalized to the average density of O atoms, averaged over both z directions, and plotted as a function of z) during several 2-ns time intervals after the beginning of the 2-nm-diameter pore simulation. (b) Cumulative "breakthrough flux" of tagged water O atoms in the same system, averaged over both directions and normalized to pore cross-section area, plotted as a function of time since the beginning of the MD simulation.

hydrophobic cylindrical nanopores with radii of 3 Å or more, water diffuses more rapidly than in bulk liquid water: $\delta \sim 1$ to 3 (Lynden-Bell and Rasaiah, 1996; Beckstein and Sansom, 2003).] The diffusion coefficients calculated here are consistent with the finding that diffusion occurs more slowly in silica gel layers than in bulk liquid water (Cailleteau et al., 2011). If we assume that silica gel layers have straight cylindrical pores with diameters of 1 to 2 nm, a porosity $\phi = 0.2 \pm 0.1$ [based on the value of 0.2 used by Ferrand et al. (2006)], and a geometric factor $G = 4.5 \pm 1.5$ [the theoretical value being $G \geq 3$ for a network of straight cylindrical pores (Dykhuizen and Casey, 1989)], we can estimate the range of possible values of the effective diffusion coefficient ($D_e = \phi\delta/G \times D_0$) of water in these gel layers as $D_e = 3.5 \times 10^{-12}$ to 1.2×10^{-10} m^2 s^{-1}.

3.3.3 Intrinsic proton affinity of silica-water interfaces

Bond-valence models are routinely used to predict the intrinsic pK_a values of surface O atoms from their molecular-scale coordination at mineral-water interfaces (Hiemstra et al., 1996; Bickmore et al., 2004; Bourg et al., 2007; Machesky et al., 2007). These models are based on the hypothesis that the pK_a values of surface O atoms correlate with the "valence oversaturation" of these atoms, defined as $S = (V + \Sigma s)$, where V is the formal valence of the oxygen atom (-2) and s is the bond valence contributed by each cation that forms a covalent or hydrogen bond with the O atom under consideration. For surface silanol O atoms (denoted Oh) in our simulated systems, $\Sigma s = s_{Si} + s_H + s_{H\text{-}bond}$, where s_{Si} and s_H are the bond valence contributions of Si and H atoms bound to the O atom under consideration in a >SiOH group, and $s_{H\text{-}bond}$ ($= s_{H\text{-}bond,silanol} + s_{H\text{-}bond,water}$) is the bond valence contributed by H-bonds from nearby silanol groups and water molecules. To a first approximation, all surface Oh atoms in our simulations have identical s_{Si} [= 1 (Hiemstra et al., 1996)] and s_H values (they all form a covalent bond with a single H atom, with a O-H bond length of 1 Å imposed by the CLAYFF model); therefore, their relative acidity is determined by $s_{H\text{-}bond}$. To evaluate $s_{H\text{-}bond}$ for each Oh atom in the 2-nm-diameter pore system, we calculated the radial distribution functions (RDF) of water H and silanol H atoms near each Oh atom; then, we multiplied each RDF by the relationship between H-bond length ($r_{H\text{-}bond}$) and

bond valence proposed by Machesky et al. (2007) [$s_{H\text{-}bond} = 1.55 - 1.06\ r_{H\text{-}bond} + 0.186\ r_{H\text{-}bond}^2$]. Finally, we integrated the resulting function from r = 1.4 to 2.4 Å (Machesky et al., 2007) to calculate $s_{H\text{-}bond,silanol}$ and $s_{H\text{-}bond,water}$ for each surface Oh atom.

The resulting cumulative distribution of $s_{H\text{-}bond}$ values is shown in Figure 3-5 for three regions of our 2-nm-diameter nanopore: pore walls (z = 67 to 123 Å), external surfaces (r > 12 Å), and the "edge" region near the pore entrance. Evidently, Oh atoms on the pore walls of cylindrical silica nanopores have less "valence oversaturation" than Oh atoms located on flat silica surfaces; therefore, they should be less acidic. The excess valence of edge Oh atoms is even lower, because the lower tendency of these atoms to receive H-bonds from nearby silanol groups is incompletely compensated by their greater tendency to receive H-bonds from water. The average difference between the $s_{H\text{-}bond}$ values of Oh atoms on pore walls and on external surfaces is 0.023 v.u. (valence units). Previous studies suggested that a 0.05 difference in S translates to approximately a unit difference in intrinsic pK_a (Hiemstra et al., 1996); therefore, our results suggest that the average intrinsic pK_a value of silanol sites in 2-nm-diameter nanopores is about 0.5 pH units higher than on flat silica surfaces. If we consider only the 5 % of silanol sites that have the highest $s_{H\text{-}bond}$ values (i.e., the sites that are the most likely to undergo the deprotonation reaction >SiOH $\Leftrightarrow$ >SiO$^-$ + H$^+$), the average difference in valence oversaturation increases to 0.61 v.u., which corresponds to a difference in intrinsic pK_a value of about 1.2 pH units.

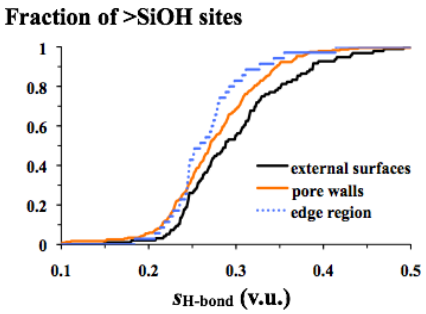

Figure 3-5. Cumulative distribution of the $s_{H\text{-}bond}$ values of silanol sites. Sites are located on the pore walls, external surfaces, or edge regions of the 2-nm-diameter silica nanopore.

In summary, we carried out molecular dynamics (MD) simulations of water in idealized silica gel layer nanopores (cylindrical pores with 6 nm length and 1 or 2 nm diameter) in order to determine how strongly the properties of nanoconfined water differ from those of bulk liquid water. We found that water diffusion coefficients in these idealized nanopores are 10 to 50 % of the diffusion coefficients of bulk liquid water. We also found (a result never previously reported, to our knowledge) that the intrinsic acidity constants of silanol functional groups (>SiOH) on curved nanopore walls should be lower than the intrinsic acidity of otherwise identical groups on flat silica surfaces.

4 MOLECULAR DYNAMICS CREATION OF BULK GLASS, GLASS SURFACES AND GEL-LAYERS

4.1 Problem

This modeling effort is designed to first generate multicomponent glass, surface, and gel structures through the use of molecular dynamics simulations, and then validate these structures with experimental data whenever possible. Representative multicomponent glass surface structures (e.g., Si-Al-O-Na, Si-B-O-Na, and Si-Al-B-O-Na) will be passed to P. Zapol (ANL) to determine from first principles the bond-breaking activation barriers for the various types of bonds found on the glass surface structures in the presence of H_2O. Representative gel structures from different initial glass compositions will be provided to I. Bourg (LBNL) for diffusion studies. Using this approach, both the diffusive transport parameters and the calculated activation energy barriers will be calculated using the same glass "standards" carefully designed through molecular dynamics models and validation (see Figure 4-1).

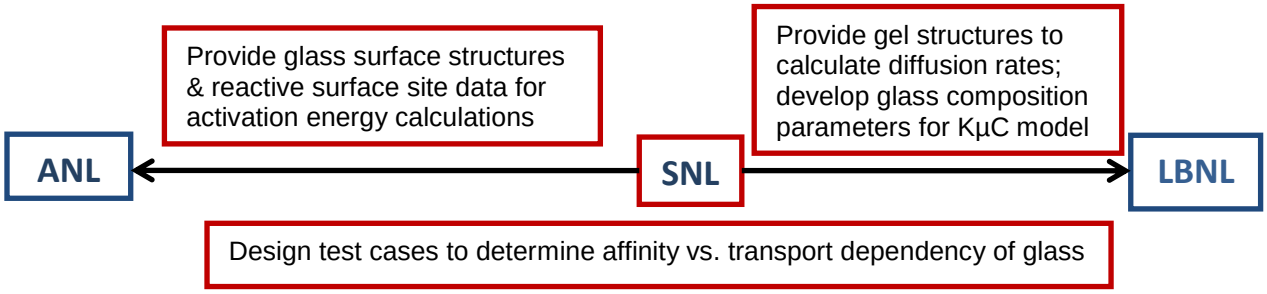

Figure 4-1. Development of internally-consistent mechanistic parameters for multicomponent glass degradation from molecular models.

This research is expected to help address the following questions: how does the glass composition influence long-term glass dissolution rates? How are changes in glass composition reflected in the glass surface? How do changes in surface site types and densities influence glass dissolution rates? Bulk 2-, 3-, 4-, and 5-component glass structures will be created through molecular dynamics simulations. Modeled glass compositions will be based on glasses that have been or will be characterized by ^{27}Al and ^{29}Si MAS-NMR data such as that reported by Pierce et al. (2010) for multicomponent (B, Al, Si, O, Na) glasses with compositions representative of nuclear waste glasses. These selections will allow for validation of the calculated bulk glass and surface structures.

Simulated glass surfaces will be hydroxylated using several different approaches. The calculated surface site density will be compared to that determined by NMR studies for different glass compositions. Hydroxylated glass surface models will be used to calculate activation energy barriers for different potential network-breaking reactions and to evaluate if the calculated highly-reactive sites are consistent with those proposed through NMR studies (e.g., Washton et al., 2008).

Molecular dynamics simulations will also be used to address questions regarding the formation and structure of gel layers at the glass-water interface: does bulk glass composition influence gel

structure? What role does condensation play in gel formation? How does this impact the transport of ions and water through the gel? One observation from experiments conducted on aluminosilicate mineral and glass dissolution is that the gel thickness varies as a function of pH and solid composition. For some compositions, no gel layer is observed at all (e.g., Hamilton et al., 2001). To determine if the gel structure can be derived from the condensation of a leached layer consisting only of silica, Mellott (2003) performed some preliminary molecular dynamics calculations to investigate how a leached layer might condense to form a gel-like structure. The calculated ratio of Q species (i.e., Q^1, Q^2, Q^3, and Q^4) in the condensed layer closely matched ^{29}Si MAS-NMR data, suggesting that condensation may play a key role in gel formation.

We will expand upon this research in order to investigate how different glass compositions and structures may result in different gel structures and thicknesses. The approach used by Mellott (2003) will be compared to more rigorous calculations performed with a reactive force field (Garofalini, 2001). Calculated gel structures for different starting glass compositions will be compared to each other as well as to available NMR data. The ratio of open versus closed porosity for calculated gel structures will be determined. Several models will be passed to I. Bourg (LBNL) to calculate apparent diffusion and transport rates of water and ions through different gel layer structures.

4.2 Methods

An intensive literature review was performed to determine how glass model structures and surfaces are generated using molecular dynamics simulations, compare the force field models available for glass simulation, and find experimental data to use for validating the simulated glass structures.

4.2.1 Designing Glass Surface Structures

Several different approaches to annealing bulk glasses have been used in the molecular modeling community. One major concern has been that the cooling rate/quenching rate in simulations is much faster than in experiments and could lead to different structures than observed. Another concern has been that the annealing cycle used may impact surface site density (Cruz-Chu et al. 2006). One approach used for SiO_2 glass is to use a non-linear cooling schedule (Della Valle and Andersen (1992). Another approach for SiO_2 glass used by Du and Cormack (2005) is to gradually heat the glass to 6000K to remove the memory effect of the initial configuration, and then cool the simulation cell down gradually to 300K with a nominal cooling speed of 10K/ps. Generating a good surface structure for the glass involves several steps: (1) add a vacuum slab to the bulk glass, (2) immobilize 25% of the glass and re-anneal the remaining 75% of the glass and glass surface, (3) relax the system at 300K, and (4) increase the immobile glass section to 50% and allow further relaxation of the near-surface and surface atoms. This process is illustrated in Figure 4-2. Figure 4-3 provides an example of using this technique for creating a silica glass surface starting with the regular crystalline structure of cristobalite as an initial configuration. The SiO_2 glass structure and surface are generated using the force field CLAYFF (Cygan et al., 2004). The glass structure is characterized by 4-fold tetrahedra of silica with no non-bridging oxygens within the bulk structure.

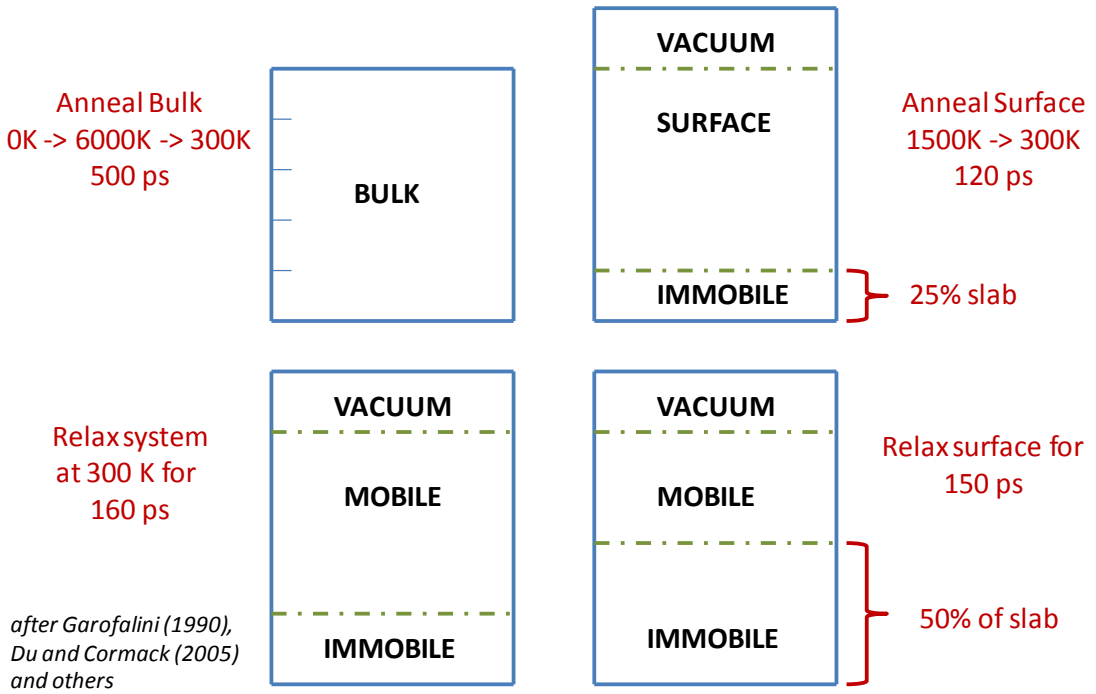

Figure 4-2. Schematic for Creating Glass Surface.

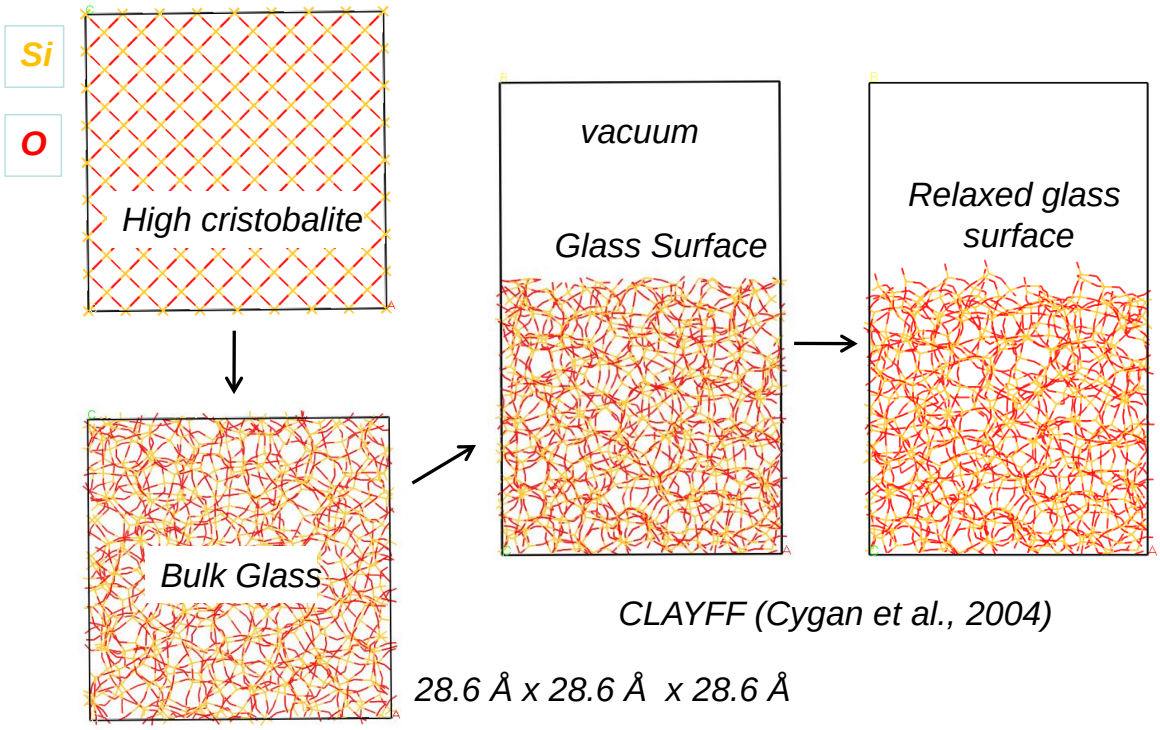

Figure 4-3. Illustration of SiO_2 Glass Surface Construction

Several different approaches have also been used to hydroxylate an amorphous SiO_2 surface. Leed and Pantano (2003) added –OH to all surface Q^3Si and –H to all non-bridging oxygens (NBO) at the surface. They assumed that H_2O adsorption occurs after reconstruction and found that hydroxylation eliminates the highest energy adsorption sites. Du and Cormack (2005) also added –OH to all surface Q^3Si, -H to NBOs, and also opened any two-member rings residing on the glass surface. Then the hydroxylated surface was relaxed at 300K for 100 picoseconds. A third approach was used by Mahadevan and Garofalini (2008) who developed a dissociative H_2O potential, such that water molecules will dissociate to hydroxylate the surface. Figure 4-4 illustrates how water dissociates and migrates into a porous silica structure using this force field.

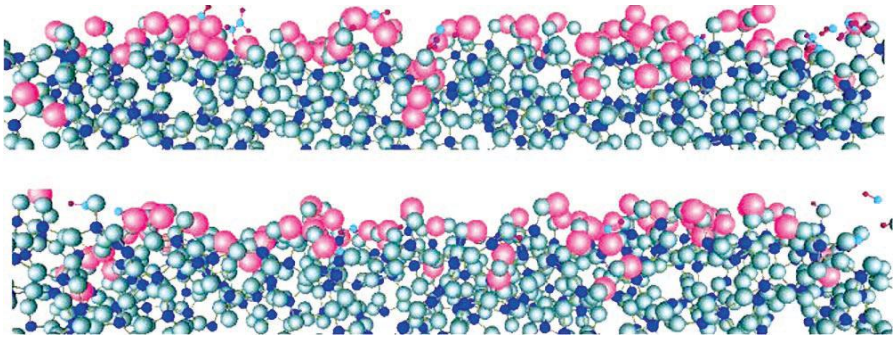

Figure 4-4. Water molecule reaction and diffusion with a silica surface.
Taken from Mahadevan and Garofalini (2008).

4.2.2 Glass Force Field Selection

In order for classical force field simulations to be successful, an appropriate force field model that can address our questions regarding multicomponent glass dissolution is required. Available force field models for multicomponent glasses have been reviewed. A summary of the force fields used to simulate multicomponent glass structures and the interaction of glass surfaces with water are provided in Table 4-1 and Table 4-2 respectively. The choice of interatomic potentials is of fundamental importance for the accuracy of simulated physical and chemical properties such as structure, elastic constants, heat capacities and other thermodynamic properties (Pedone et al., 2006). Several interatomic potentials are available in the literature for silica glass and silica polymorphs (Van Beest et al., 1990; Duffrene and Kieffer, 1998; Demilrap et al., 1999; Vashishta et al., 1990; Takada et al., 2004). However fewer potentials are available for multicomponent glass systems and there have not been many efforts to provide generalized self-consistent force fields that are capable of modeling the structures, mechanical, and chemical properties of silica-based glasses with different compositions. From our review of available force fields, three stand out as candidates for the development of an internally consistent database of glass surface and gel structures for use to investigate both reaction and diffusion properties for glass dissolution.

The first force field that is worthy of consideration was developed by Delaye and Ghaleb (1996) to simulate a nuclear waste glass matrix. As in previous simulation studies of the structure of simple glasses (e.g., Soules, 1979; Soules and Varshneya, 1981), potentials of the Born-Mayer-Huggins (BMH) form were used to represent a glass comprising the major components of a nuclear waste glass ($SiO_2 + B_2O_3 + ZrO_2 + Al_2O_3 + Na_2O$ (+ CaO)). Three-body potentials were

applied to O-Si-O, O-B-O and Si-O-Si triplets. The local environmental structures showed overall agreement with experimental results and the simulated densities, thermal expansion coefficients and viscosities of the simulated glasses were on the same order of magnitude as experimental data. Delaye et al. (1997) used this force field to examine a suite of nuclear waste glass compositions and found that the gradual incorporation of boron into the silicate network, the attraction of sodium atoms by four-coordinate boron and changes in the distances between atoms in the glass structure were reproduced by the force field model. In addition, boron-enriched segregation zones were observed in a composition not containing aluminum. Additional work by this French group includes combined multiple-quantum magic angle spinning (MQ-NMR) spectroscopic and molecular dynamics studies to examine the Na environment in several two- and three-component glasses (Angeli et al., 2000a) and changes in Al-O-Si angle with increasing Ca content (Angeli et al., 2000b). Abbas et al. (2003) used this same force field model to compare the structural properties of bulk glass with a glass surface. The simulations predict the migration of alkali cations toward the surface, lower coordination numbers for trivalent elements in the subsurface layer, oxygen enrichment in the outer layer, and larger tetrahedral ring structures on the surface. The main disadvantage of pursuing the use of this force field to investigate the degradation of nuclear waste glass is that, to our knowledge, it has not yet been developed to look at the interactions of glass with water.

The second force field model to be considered is that of Pedone et al. (2006) who developed a generalized self-consistent force field that is able to model both the structures and mechanical properties of silica-based glasses with different compositions. To produce a coherent set of potential functions, these researchers performed empirical fitting to structural and mechanical properties of a large set of crystalline oxides. The potentials developed in this work consist of three terms: a long-range Coulomb potential, a short-range Morse function, and a repulsive contribution (C/r^{12}). The resulting potential is given by:

$$U(r) = \frac{z_i z_j e^2}{r} + D_{ij}\left[\left\{1 - e^{-a_{ij}(r-r_0)^2}\right\} - 1\right] + \frac{C_{ij}}{r^{12}}$$

A rigid ionic model with partial charges is used to handle the partial covalency of silicate systems in order to model the quenching of melts and structures and mechanical properties of glasses. A core-shell model might provide more accurate results for surfaces, but would require a shorter time step and lead to computationally more expensive quench simulations.

This force field has been parameterized to include numerous glass components including many of importance in nuclear waste glasses (Na_2O, CaO, Al_2O_3, SiO_2, and ZrO_2). Boron force field parameters have also been developed using this potential form (Cormack, *pers. comm.*) However, to our knowledge, this force field has neither been used to study glass surface structures nor combined with a water model to examine glass surface hydroxylation or other interactions between glass surfaces and water.

In earlier papers by the same group (Du and Cormack, 2005; Zeitler and Cormack, 2006), surface hydroxyl-silicon and hydroxyl-phosphorous potentials were developed to study the hydroxylation of silica and phosphosilicate glasses. These potentials include a short-range interaction described by a Buckingham equation, a potential function for the hydroxyl group that

has the Coulomb-subtracted Morse form, and a three-body term introduced to reproduce the Si(P)-O-H bond angles on glass surfaces. The surface structures were used successfully to investigate the energy of chemisorption of water on different surface sites and to determine the OH coverage of glasses.

The third force field that shows promise for our study is the reactive force field of Garofalini (2001). From the beginning, this force field was developed to investigate glass surface structures and the interaction of water with glass surfaces. It now includes parameters for Si, Al, and B, and also allows for breaking glass network bonds between Si-O, Al-O and B-O (Garofalini, *pers. comm.*) by reaction with water molecules. This force field has been demonstrated to successfully reproduce bulk glass and hydroxylated surface structures, but is not entirely reliable for calculating the energetics of these systems. Mahadevan and Garofalini (2007, 2008) have developed a new dissociative water potential to improve upon the previous force field model. However, this new potential has not yet been developed to work with Al and B.

Because we are, in the long term, interested in simulating multicomponent glass surfaces, determining the hydroxylation of these surfaces in contact with water, and generating interfacial gel structures, we will start by validating simulated glass structures with the Garofalini (2001) force field model against NMR glass structure data. Postprocessors to calculate glass ring structures and the number of different Q species present in MD-simulated bulk glass structures will also be evaluated. Molecular dynamics software (e.g., LAMMPS, Plimpton, 1995; DL-POLY, Smith and Forester, 1996) will be selected based on compatibility with the force field model.

4.2.3 Experimental Validation

Two suites of multicomponent glass studies have been chosen as good validation studies for our multicomponent glass simulations. The first suite of glasses are Si-Al-Na-Ca-O glasses with SiO_2:Al_2O_3 ratios ranging from 50:50 to 70:30, and CaO:Na_2O ratios ranging from 10:90 to 20:80 studied by Mellott (2003). The bulk glass structures were determined with UV-Raman spectroscopy, IR-absorption spectroscopy and ^{29}Si MAS-NMR. Surface layer structures were also determined after acidic dissolution with ^{29}Si MAS-NMR. Some of the glass compositions in this series lead to "protective" surface layers while other compositions did not. Secondary ion mass spectrometry (SIMS) data showed that the gel layers are pure silica and that the interface between the glass surface and the gel layer is very sharp (Figure 4-5A).

Mellott (2003) also used molecular dynamics simulations to test the hypothesis that the silica gel layer forms strictly from the condensation of a residual silica framework from the original glass structure. That is, the formation of the gel layer does not involve surface precipitation or other processes. The approach used by Mellott (2003) included the following steps: (1) create a multicomponent glass structure using molecular simulation, (2) remove all atoms in the structure that are not part of a Si-O-Si framework, (3) hydroxylate all non-bridging oxygens, (4) allow this structure to relax using molecular simulations, (5) periodically stop the simulations, and

Table 4-1. Force field models for glass.

Composition	Form of Potential	Authors
Na, K, Ca, Si, B, O	Modified BMH used by Busing w/o dispersion terms	Soules (1979)
SiO_2, $AlPO_4$	Buckingham form known as BKS	Van Beest, Kramer, & van Santen (1990)
Al, O	Modified BMH	Blonski and Garofalini (1993)
Li, Cs, B, O	BMH	Verhoef & den Hartog (1995)
Mg, Ca, Al, Si, O	Modified BMH used by Busing w/o dispersion terms	Okuno & Kawamura (1995)
Na, Ca, Al, Si, B, Zr, O	BMH	Delaye & Ghaleb (1996)
Na, Ca, Al, Si, B, O	BMH – improvement on D&G (1996)	Abbas et al. (2003); Cormier et al. (2003)
Na, Si, O	Buckingham	Du and Cormack (2004)
Al, O	Buckingham	Adiga et al. (2006)
Na, Ca, Si, Al, O, Zr	Morse function with partial ionic charge model	Pedone et al. (2006)

Table 4-2. Force field models for glass-water interaction.

Composition	FF for Glass	FF for –OH and H_2O	Authors
Si, Na, H_2O	BMH	Shell model for H_2O -OH: Morse potential	Leed and Pantano (2003)
Si, O, Si-OH, H_2O	Buckingham (Teter's)	3-body term for Si-O-H; Coulomb subtracted Morse potential for –OH group	Du and Cormack (2005)
Si, O, Si-OH, H_2O	BMH + 3 bond angle terms	Rahman, Stillinger & Lemberg form for Si-H, O-H, and H-H	Feuston and Garofalini (1990)
Si, O, Si-OH, H_2O	Modified BMH + 3-body potential	Modified BMH + 3-body potential	Litton and Garofalini (2001)
Si, O, Si-OH, H_2O	Modified BMH + 3-body potential	Modified BMH + 3-body potential	Garofalini (2001)
Si, O, Si-OH, H_2O	Modified BMH + 3-body potential	New dissociative H_2O model	Mahadevan and Garofalini (2007)

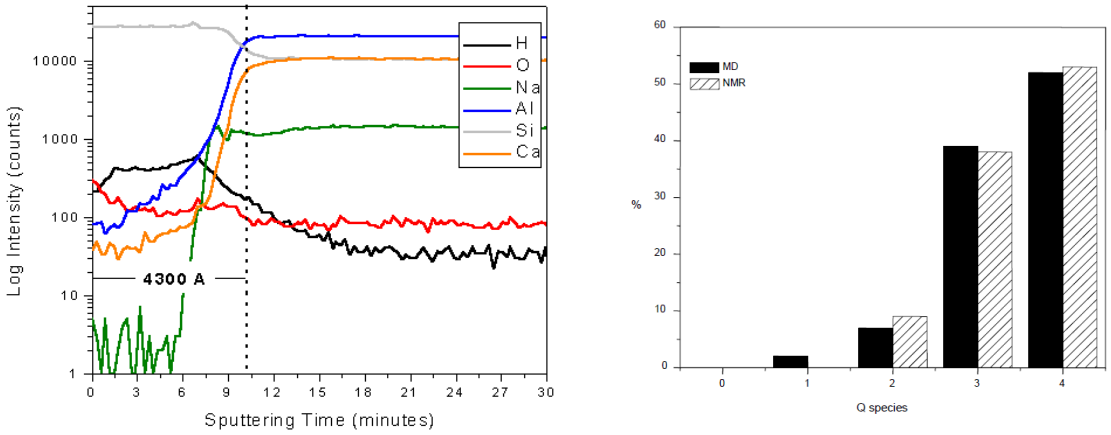

Figure 4-5. Ca-Na-Al-Si-O glass dissolution studies.
A. SIMS data for a reacted glass at pH 1 for 10 hours. The distance 4300 Å represents the thickness of the gel layer on a 20 mol% CaO glass. Note that this layer is enriched in Si and H and depleted in Al, Ca, and Na. B. A comparison of the Q distribution of Si-species in the surface layer determined by NMR and through MD simulations (*fr. Mellott, 2003*).

"condense" the gel through the reaction 2 SiOH → Si-O-Si + H_2O wherever two SiOH groups are close together. The results of this simulation study were compared to data from ^{29}Si MAS NMR on the ratio of Q^1, Q^2, and Q^3 silica present in the gel structure. This comparison, illustrated in Figure 4-5B suggests that the localized condensation of a hydroxylated/leached structure is sufficient to explain the formation and structure of the gel layers.

The second suite of data that has been selected for use in validation is the suite of glasses along the nepheline ($NaAlSiO_4$)-malinkoite ($NaBSiO_4$) join studied by Pierce et al. (2010). Pierce et al. (2010) used ^{27}Al and ^{29}Si MAS-NMR spectroscopy to analyze the structure of unreacted glasses prior to conducting single-pass flow-through (SPFT) experiments under neutral to alkaline conditions. Structural properties for the glasses along this join that were determined spectroscopically include the coordination numbers of Al, Si, and B in the glasses, the distribution of three-fold boron between ring and non-ring moieties and the changes in boron coordination as a function of B/Al ratio. Through coordination with Pierce (ORNL) and Mueller (PNNL), we will collect NMR data on the gel layers produced on these glasses after the experiments to validate the simulated gel compositions and structures created through molecular modeling.

Finally, through collaboration with Mueller (PNNL) and Washton (PNNL), we will validate the structure of our glass surfaces with NMR studies that are specifically designed to probe the reactive sites on glass surfaces. Washton et al. (2008) measured the number of reactive sites on aluminosilicate glass surfaces with ^{19}F NMR spectroscopy using a fluorine-containing TFS [(3,3,3-trifluoropropyl)dimethylchorosilane] probe molecule. The TFS-reactive T-OH species on the glass surface are known to be non-H-bonded Q^3 groups, and may represent loci that are accessible to and affected by proton-mediated dissolution. The rates of dissolution for the suite of aluminosilicate glasses studied appear to be roughly correlated with the number of these

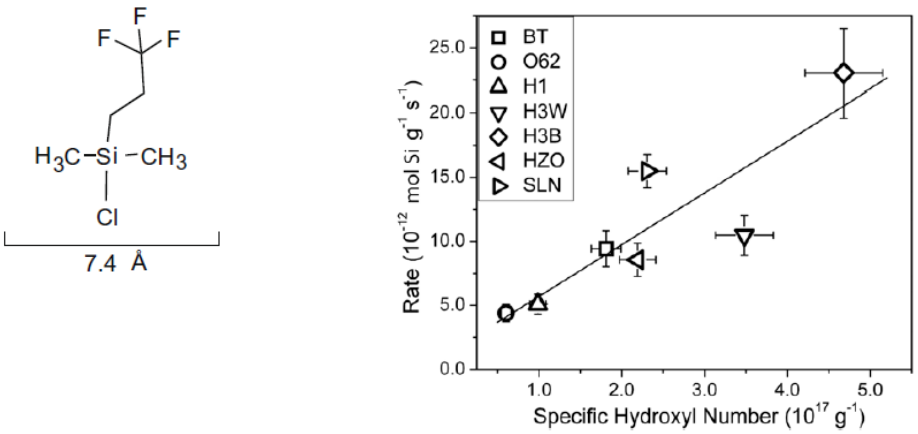

Figure 4-6. TFS-probe results on aluminosilicate glasses.
A. Schematic of TFS probe ((3,3,3-trifluoropropyl)demethylchlorosilane)) molecule. B. Correlation between the number of hydroxyl groups on different glass surfaces determined by TFS probe studies and glass dissolution rates.

groups on the glass surfaces (Figure 4-6). Regardless of the function of these sites in the dissolution process, the number of isolated Q^3 groups on our simulated surfaces can be compared to the number detected through this NMR method to validate our glass surface structures. The reactivity of these surface sites will then be compared to the reactivity of other surface site types through first-principle based calculations performed by P. Zapol at ANL.

4.2.4 Overall Approach

A matrix of molecular dynamics calculations will be performed to develop glass structures and surfaces. First, we will simulate SiO_2 glass and glass surfaces. Then we will create a suite of borosilicate glasses with different B:Si ratios. These simulated glasses may be generated using two different force field models (e.g., Pedone et al., 2006 and Garofalini, 2001) to determine which model best reproduces observed BO_3:BO_4 distributions. Then we will either develop models for a suite of (Na,Ca)-aluminosilicate glasses analogous to those studied by Mellott (Alfred University) and Pantano (PennState-NEUP), or move forward to developing models for the glasses along the nepheline ($NaAlSiO_4$)-malinkoite ($NaBSiO_4$) join studied by Pierce et al. (2010). The choice of simple system glasses that will be studied may be revised to better coordinate with ongoing NMR research conducted by K. Murphy, C. Pantano, and K. Mueller (Nuclear Energy – University Program; PNNL and PSU).

Each simulated glass surface will be created through numerous annealing and relaxation steps as recommended by Garofalini (1990) and Du and Cormack (2005). Statistical studies will be performed to determine if the simulated glass surface areas are sufficient to be representative of each glass composition. Surface hydroxyl groups will be added to these surfaces according to the method of Leed and Pantano (2003) and Du and Cormack (2005) for silica glasses. This approach will be expanded for multicomponent glasses. For comparison, surface hydroxyl groups will also be created using the dissociative H_2O potential of Garofalini (2001).

Gel structures will be designed using the simple approach developed by Mellott (2003). While this approach is somewhat simplistic it will lead to quick results that can be used to determine if

a more rigorous quantitative approach should be implemented. Gel structures will also be developed using the reactive force field model of Garofalini (2001) which is capable of reproducing Na-Si-Al-B-O glasses successfully (*pers. comm.*). This more rigorous approach will allow for calculations involving water dissociation, Si-OH bond-breaking and condensation (Si-OH + Si-OH → Si-O-Si + H_2O), and should enable us to dynamically reproduce gel-like structures from pristine glass surfaces.

Several assumptions are made in defining this task. First, it is unlikely that we will be able to use molecular dynamics simulations to examine glass structures and surfaces of 10 to 15 components directly comparable to actual nuclear waste glasses. Therefore, we are assuming that the major constituents (Al, Si, B, O, Na) are the critical components to consider. This assumption may need to be re-evaluated. For example, Zr is not present in large quantities in nuclear waste glasses, yet appears to have a very important role in controlling glass dissolution rates (e.g., see Cailleteau et al., 2008).

A second assumption is that currently available classical (e.g, Pedone et al., 2008) and reactive force field models (Garofalini, 2001; Mahadevan and Garofalini, 2007; 2008) can effectively be used to model the multicomponent glass structures and surfaces proposed for study. There is a possibility that additional force field development will be required.

A third assumption is that sufficient experimental data for model validation is available for the glass compositions we will study or that it will be collected during the course of this project.

4.3 Expected Results and Collaborations

This task lies at the center of the program as is illustrated in Figure 4-7 (the same as Figure 1-4). It is anticipated that the glass surface and gel structures created in this task will provide the foundation for studying hydrolysis of multicomponent glass networks of different compositions and diffusion transport through gel structures. These modeled structures will also provide information regarding glass surface structures as a function of glass composition such as (a) the ratio of Q^1, Q^2, Q^3 sites, (b) the number of Si, Al, and/or B surface sites, (c) the variance in ring structures at glass surfaces. The modeled structures will complement the collection of NMR and other spectroscopic data, providing a second line of inquiry into glass and gel structures.

The modeling methodology developed during the course of this research includes: (a) the selection of a force field, (b) the surface annealing procedure, and (c) statistical tests to confirm that simulated glass surfaces are of adequate size to represent the various structures that form on a non-periodic surface, will ultimately providing a protocol for future computational studies of this nature, that may be used to evaluate new glass compositions of greater durability.

Calculations to determine how initial glass compositions and structure influence gel formation will address one key unknown in our understanding of glass dissolution mechanisms. Although all gel layers are primarily silica, some have been observed to protect the bulk glass from dissolution, while others do not have this capability. Understanding how and if the initial glass framework dictates the gel structure and its impact on glass dissolution is critical to designing appropriate glass waste forms.

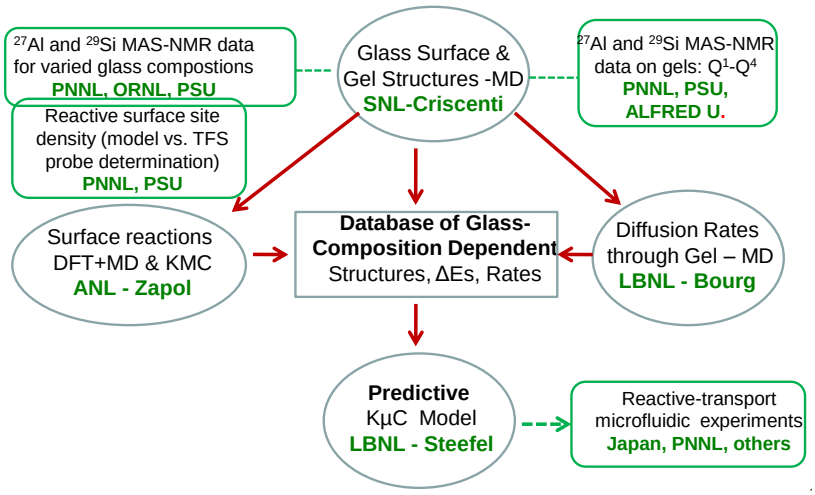

Figure 4-7. Flow chart illustrating coordinated modeling and experimental program effort.

This research will provide fundamental information on how the starting composition of a glass waste form impacts glass dissolution in numerous ways: (1) glass surfaces generated by molecular dynamics simulations will be used as the starting point to determine the activation energy barriers associated with network-breaking given different glass networks of different structures and composition, and (2) the creation of gel-like silica structures from different glass compositions, will provide information regarding the range of silica gel structures that may form at glass surfaces and the nature of their consequent porosity and diffusive characteristics.

In combination with P. Zapol's and I. Bourg's research, this work should lead to the development of a kinetic database for KμC, Steefel's microcontinuum model. This database will include activation energies and diffusivities, which will enable predictive reactive-transport calculations of glass dissolution that include both reaction and transport, and can be used for sensitivity studies to determine the relative importance of both processes over the life-time of nuclear waste glasses.

Interactions between this task and others include collaborations with (1) K. Murphy, C. Pantano, and K. Mueller to coordinate the simulation of glass structures that are simultaneously being investigated by NMR spectroscopy, (2) P. Zapol involving the handoff of glass surface structures for first principles calculations of activation energy barriers, (3) I. Bourg involving the handoff of gel surface structures for diffusion studies, and (4) C. Steefel to create a database of kinetic reaction and transport parameters that can be used with KμC.

5 KINETIC MICRO-CONTINUUM (KμC) MODEL

5.1 Introduction

A new Kinetic Micro-Continuum (KμC) model for glass corrosion has been developed that avoids *a priori* assumptions about what the rate-limiting steps are in the overall corrosion process. In contrast, the GRAAL model (Frugier et al., 2008; Cailleteau et al., 2008), assumes a diffusion-limited glass corrosion rate. The coupling of transport and chemical processes in KμC may result in the identification of a rate limiting step (e.g., diffusion or surface reaction), or it may predict that there is a mixed rate control depending on the parameters and processes needed to describe the available data. The KμC model provides a flexible approach in which individual parameters and processes are tunable, but in every case coupled within an overall dynamic framework. In the current implementation of the KμC model, borosilicate glass is divided into two principle components: a silica-rich component that can undergo kinetically-controlled dissolution, recrystallization and densification, and a second component consisting of all the other glass constituents. The latter may dissolve at a different rate than the silica-rich component, making it possible to capture the incongruency of the corrosion process at low pH (e.g., Inagaki et al., 2009; Geisler et al., 2010). Whether a passivating layer forms in the KμC model depends on the relative rates of (a) silica recrystallization and densification and (b) leaching of individual glass constituents. This model does not provide a "universal model" because borosilicate glass dissolution rates and reaction products differ depending on the environmental conditions.

5.2 Implementation in the KμC Model

The KμC is based on the code CrunchFlow, which is a general purpose multicomponent reactive transport simulator developed at Lawrence Berkeley National Laboratory and other institutions (http://www.csteefel.com/CrunchPublic/CrunchFlowIntroduction.html). As such, formulations for transport and kinetically controlled reactions are based on the capabilities found there, although modifications are possible.

5.2.1 Diffusion of Water and Ion Exchange in the Glass

CrunchFlow assumes that an aqueous phase is present throughout the domain, so it is necessary to model water diffusion as if it were a trace component that diffuses through the water into the glass. In this way, the diffusivity of water can be set at any value desired. The rate of network-modifying cation release, R_{ex}, (and potentially hydrolysis) can then be calculated by multiplying the rate constant, k_{ex}, (and any other factors in the rate law) by the fictive water concentration:

$$R_{ex} = C_{H_2O} k_{ex}. \tag{5.1}$$

This formulation results in a dissolution rate that is controlled by the diffusion of water into the glass if the rate constant used is larger than the diffusion coefficient for water in glass. That is, if the water diffusion front has not penetrated a certain distance, then the concentration (used as a proxy here for water activity) is zero or very low, resulting in a low rate of exchange or hydrolysis.

5.2.2 Hydrolysis Reactions

In the KμC model, it is possible to consider either

1. a single glass phase that dissolves congruently with or without a chemical affinity control (any mineral phase can be used for this affinity control, although of course it needs to involve chemical constituents present in the glass), or
2. multiple glass phases corresponding to end-members treated at this stage as a mechanical mixture. The mechanical mixture is designed to have the silica-rich portion of the glass dissolve at a different rate from the non-silica rich portion. It would be possible to consider the activities of the end-members such that they affect the activities of the other end-members as either an ideal or non-ideal solid solution, but so far this has not been implemented in the model. This approach would also apply if the glass was phase separated.

If a chemical affinity term is included, it is typically a "cross-affinity" expression in which the rate of glass corrosion scales with the departure from equilibrium with respect to a phase like amorphous silica. Because glass is a metastable phase, a "Cross-Affinity Phase" such as amorphous silica, is assigned to define a pseudo-equilibrium state between a glass component and the aqueous solution. A linear TST expression for the rate of dissolution of the glass, R_{glass}, of the following form is often used (Grambow and Müller, 2001):

$$R_{glass} = -A_{glass} k_{glass} \left(1 - {Q_{CAP}}/{K_{CAP}}\right), \tag{5.2}$$

where Q_{CAP} and K_{CAP} refer to the ion activity product and equilibrium constant for the "Cross-Affinity Phase" respectively, A_{glass} is the reactive surface area of the glass, and k_{glass} is the rate constant.

5.2.3 Silica Condensation/Recrystallization

There are at least two possible ways to simulate silica condensation in the KμC model

1. kinetically-controlled recrystallization (ripening) of the residual silica-rich glass network following incongruent glass dissolution, and
2. precipitation of a silica-rich phase following congruent dissolution of the glass phase.

To the extent that the rate of recrystallization is rapid, implying that the residual silica network is short-lived, the two approaches should be similar. However, the first option offers the possibility of differing rates or extents of recrystallization that depend on the glass composition. The first approach may be useful for simulating the boron leaching experiments described in Cailleteau et al. (2008) in which the degree of densification depended on the Zr content of the glass. Even where rapid precipitation is used to represent a silica-rich gel layer formed following congruent dissolution, it is possible to treat the ripening (and potentially densification) of this phase or phases as kinetically controlled. This allows one to consider time-dependent densification, as in the Monte Carlo modeling presented by Cailleteau et al. (2008).

Silica recondensation from the silica-rich glass network can be treated as a first order kinetic process according to

$$R_{xtl} = k_{xlt} C_{gel} \tag{5.3}$$

where k_{xlt} is the rate constant and C_{gel} is the concentration (or volume fraction) of the amorphous gel. Or the ripening rate can be made to depend on the concentration of other network-forming constituents that may be present, in which case the silica recrystallization rate, R_{xlt}, is treated as inversely proportional to the concentration of the other network formers (principally B and Al where applicable) in the glass according to:

$$R_{xlt} = k_{xlt} C_{gel} \left(\frac{k_{in}}{k_{in} + C_{NF}} \right) \tag{5.4}$$

where the last expression on the right hand side is a hyperbolic inhibition function in which C_{NF} is the concentration (volume %) of the inhibiting network former and k_{in} is the concentration of the network former at which the rate is reduced by half. Other components like Al are grouped with boron in the non-silica phase and thus play an equivalent role in inhibiting silica leaching.

5.2.4 Mineral Precipitation

Mineral precipitation in the KμC model is handled in a similar fashion to the way it is usually treated in the CrunchFlow code based on either irreversible or TST-type rate laws (Lasaga, 1981; 1984; Aagaard and Helgeson, 1982; Maher et al., 2006; Maher et al., 2009):

$$R = A_m k_m exp\left[\frac{-E_a}{RT}\right] \prod a_i^n \left[1 - exp(m_2 g^{m_3})\right]^{m_1} \tag{5.5}$$

$$g \equiv \frac{\Delta G}{RT} = ln\left[\frac{Q_m}{K_{eq}}\right]$$

where A_m is the mineral surface area, k_m is the intrinsic rate constant in units of mol/m^2/s, E_a is the activation energy (kcal/mole), Q_m is the ion activity product for the mineral-water reaction, K_{eq} is the corresponding equilibrium constant, and $\prod a_i^n$ is a product representing the inhibition or catalysis of the reaction by various ions in solution raised to the power n. In this equation, the coefficients m_1, m_2, and m_3 are adjustable parameters that allow one to fit the rate versus the departure from equilibrium. An *ad hoc* treatment of nucleation can be included by using nonlinear precipitation rate laws.

5.3 Simulating Microfluidic Reactor Experiments

Yaohiro Inagaki of Kyushu University, Japan has presented the results of a series of innovative microfluidic reactor experiments using wafers of borosilicate glass similar in composition to the French SON68 glass (Inagaki et al., 2009). Although not without some limitations and/or analytical challenges, the Inagaki approach offers the advantage that it can be (and usually is) run in flowthrough mode, making it possible to maintain steady-state fluid chemistry in the reaction cell while allowing for analysis of the chemical composition of the reactor effluent. Because a polished glass surface is used, post-mortem profiling of the glass surface perpendicular to the direction of flow can be used to provide additional constraints on the reaction mechanism involved. The design of the microfluidic reactor is shown in Figure 5-1. Depending on the flow and reaction rates, longitudinal gradients in solution composition (especially pH and silica) developed in the reactor may lead to different extents of reaction and corrosion depths along the length of the glass sample.

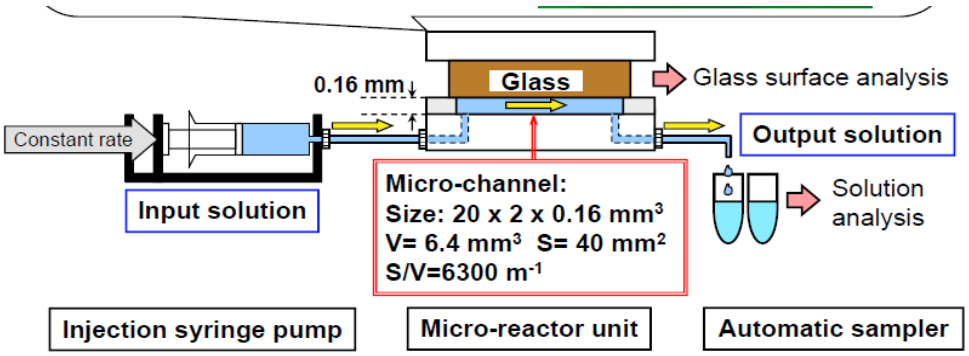

Figure 5-1. Schematic of Inagaki et al. (2009) microfluidic flow reactor.

To model the Inagaki microfluidic reactors, an analytical expression for Poiseuille flow based on flow between two parallel plates is used (e.g., Li et al., 2008):

$$u(x) = 1.5U\left[1 - \left(\frac{x}{\delta}\right)^2\right] \tag{5.6}$$

where x is the transverse distance to the center of a fracture with the origin being the center of the aperture, u(x) is the local fluid velocity within the fracture, U is the average flow velocity, and δ is the half fracture aperture. This results in the familiar parabolic velocity profile (Figure 5-2). As it uses an analytical expression that assumes fixed flow between parallel plates, the approach breaks down if the glass-water interface retreats substantially due to corrosion, or if longitudinal gradients in the extent of reaction develop to the point where the plates are no longer parallel.

By using a realistic set of molecular diffusion coefficients, it is possible to evaluate the extent of homogenization in both the transverse (x-direction) and longitudinal direction for a given flow rate and reactor geometry. This becomes an issue to the extent that it is important to know the geochemical conditions immediately adjacent to the glass surface, since these could differ from the bulk solution collected as effluent. Figure 5-3 shows the results of a Poiseuille flow and transport simulation using the Inagaki microfluidic reactor design and a flow rate of 5 µl/minute. The tracer concentration is fixed within all of the grid cells at the glass-fluid interface. Molecular diffusion accounts for the spreading and homogenization of the concentration field over the width of the reactor. In this case, the effluent actually does reflect the concentration at the glass interface. However, these results depend on the scenario considered, so the presence or absence of transverse and/or longitudinal gradients must be verified on a case by case basis.

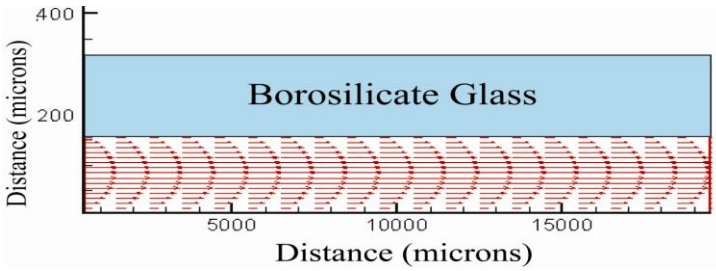

Figure 5-2. Parabolic velocity profile for Poiseuille Flow between two parallel plates.

5.3.1 Matching Effluent Chemistry

As a preliminary test of the KμC model's ability to describe the corrosion behavior at early times, we have matched the early stage effluent chemistry from the Inagaki microfluidic experiments using a two glass model (one glass consisting of silica, the other of all other network formers). In this case, the fluid flows past the polished and largely unaltered borosilicate glass surface, so early data should reflect reaction with the glass before any significant gel layers have formed or a diffusion-controlled rate is potentially applicable. The pH dependence of the glass dissolution rate at 25°C under acidic and basic conditions was taken from the microfluidic reactor data of Inagaki et al. (2009) and used in the modeling is described in

Table 5-1. The Inagaki experiments were conducted in 1 mM KCl at 25°C using a flow rate of 5 µl/min.

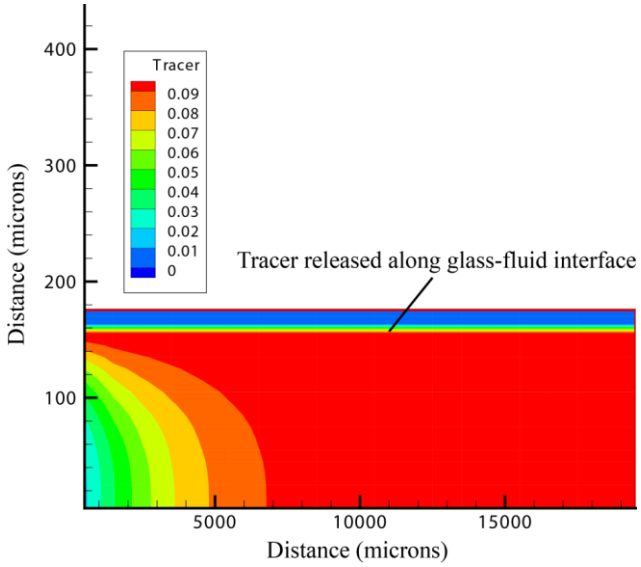

Figure 5-3. Release of a tracer along the glass-fluid interface.
The solution is homogenized at the exit of the reactor (right end). Flow is from left to right, with a total volumetric flow rate of 5 µl/min.

Identical values for these parameters were used in the modeling. The Inagaki data (Figure 5-4) show that silica and boron are released at rates that are almost an order of magnitude different at pH 3.0, while the dissolution is fully congruent at pH 8 and 11. The rates shown on the Y-axis in Figure 5-4 are normalized, with units of g/m^2/day

$$NR_i = \frac{C_i V}{\Delta t f_i S} \tag{5.6}$$

where C_i is the concentration of element i in the output solution, Δt is the sampling period, f_i is the mass fraction of element i in the glass, V is the volume of output solution, and S is the geometric glass surface area (20 mm by 2 mm = 40 mm^2).

The match obtained with the KµC model for pH 3.0 and 5.6 are shown in Figure 5-5. The gradients in solution saturation state with respect to amorphous silica do develop, but the solution remains far from equilibrium with respect to that phase in these simulations. This will not be the case in every situation, but the effluent chemistry provides a good first order indicator of conditions in the reactor given the relatively strong homogenization under these flow conditions and reactor geometry.

Table 5-1. pH dependence of early glass corrosion rates at 25°C.
Data from Inagaki et al (2009).

Glass Composition	Acidic (pH 3.0-8.0)	Basic (pH 8.0-11.0)
Silica Fraction	0.328	0.222
Non-Silica Fraction	0.500	0.222

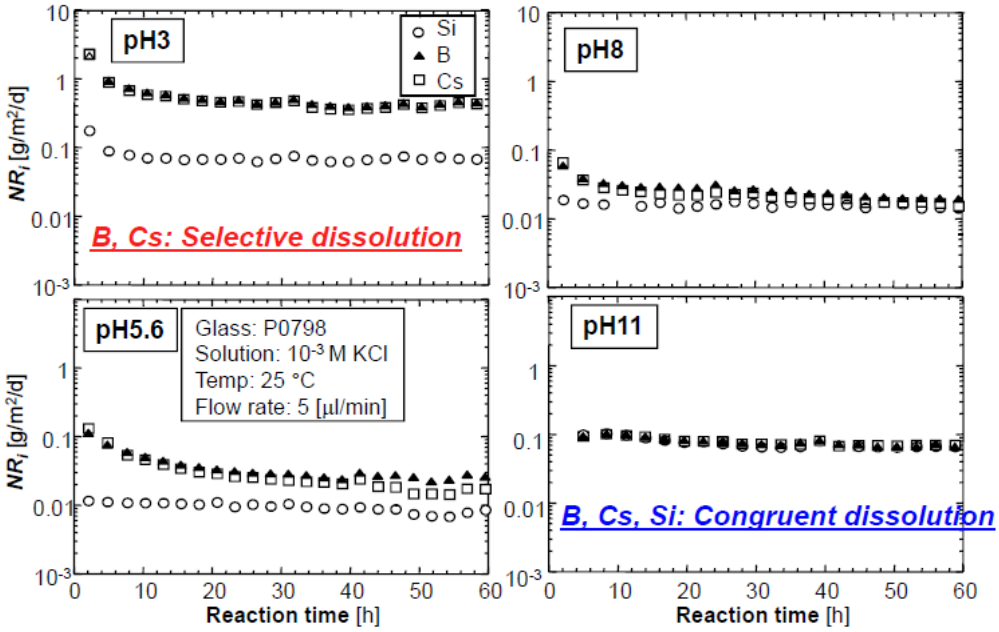

Figure 5-4. Microfluidic reactor showing release rates from glass P0798 at 25°C
(Inagaki et al., 2009).

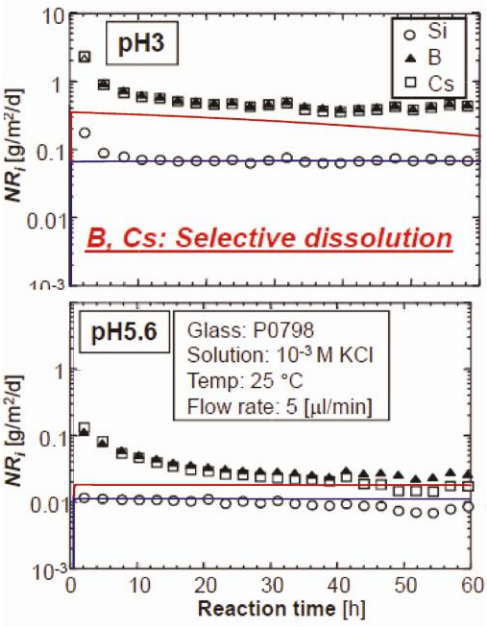

Figure 5-5. KµC model results compared to effluent data microfluidic reactor experiments at pH 3.0 and 5.6
(Inagaki et al., 2009).

5.4 Matching Secondary Ion Mass Spectrometry Profiles

While it is possible to obtain a reasonable fit of the early time corrosion behavior, it is more difficult to match the longer term time evolution of element release rates. This is presumably because a gel or other protective layer develops on the pristine glass surface as it retreats. This layer may result in a solution composition immediately adjacent to the glass surface that is different from that in the flow chamber. The extent to which the solution compositions differ depends on the diffusivity of the layer. If a low-diffusivity layer develops, as is expected for the case in which the residual glass structure recrystallizes and densifies, then the rates of interfacial reaction and diffusion are coupled.

In order to test the KμC model over longer time periods, it is useful to both match effluent chemistry for extended periods, and the corrosion profiles perpendicular to the glass-solution interface. The alteration layer formed on the glass should be analyzed in terms of both its chemical and physical characteristics, including diffusivity. A research plan to do this is under development, but for now we focus on matching the approximate corrosion thicknesses, contrasting a model in which densification results in a lower porosity and diffusivity in the gel layer with one in which it does not. For comparison, we use again the data of Inagaki et al. (2009), in this case an experiment carried out at 90°C and pH = 5.6 over 1,000 hours. The results of Secondary Ion Mass Spectrometry (SIMS) profiling show that the glass and gel have retreated a total distance of about 14 μm. After 1,000 hours, the leached layer consists of two zones, one that is 7 μm thick in which silica is preserved while boron and cesium are partly depleted, and another one that is 7 μm thick in which boron and cesium are completely leached and silica is again preserved.

Note that a simple kinetic model in which the silica and non-silica fronts retreat at different rates can be eliminated almost immediately, since this would normally result in a silica profile that is even more gradual than the non-silica (boron) spatial profile. This follows from the definition of the Damköhler II number in which the smaller the number, the broader (and more gradual) is the reaction front interface (Steefel and Maher, 2009). The lack of a silica gradient argues that the silica rich residuum is either a direct precipitate or a recrystallization product.

5.4.1 Two Glass Model

The KμC modeling described here is based on an approach in which the silica and non-silica fractions are treated as two separate glass components that are allowed to dissolve at different rates. In this formulation, the silica-rich residuum may then recrystallize at a rate that is inversely proportional to the presence of the boron network formers. The recrystallization may result in densification or little change in porosity and diffusivity. The scenario that develops depends on the density of the reaction product. If densification occurs, the formation of a Passive Reactive Interface (or PRI) is possible, although this depends in detail on what the resulting diffusivity of the gel layer and/or PRI is. The overall rate of corrosion is expected to decrease as the diffusion barrier and distance become more important with time.

Figure 5-6 contrasts the behavior of two cases calculated with the KμC model. In the first case, the porosity ratio = 1, the silica-rich residuum does not densify (Figure 5-6A), the diffusivity remains fairly high and the fronts are able to retreat at a rate largely set by the kinetics of the reaction. That is, the glass dissolution rate is not diffusion-limited. The silica gel itself dissolves under the dilute, far-from equilibrium conditions of the solution in the flow chamber. This result

agrees in general with observations that a dense silica gel layer, or PRI, does not form in dilute systems. In the second case (Figure 5-6B) the densification of the silica gel results in a lower diffusivity, forming a PRI and decreasing the advance of corrosion. Note that, in contrast to the data from Inagaki et al. (2009), the calculated silica front does not advance a significant distance from its starting position at 160 μm in this scenario. However, in agreement with the SIMS data, the silica profile obtained by summing the glass silica and the gel silica is relatively flat across the sloping boron profile. The capability of this second "Densification" case to capture the front geometries, if not the front positions, suggests that it is closer to describing the correct dissolution mechanisms. Inputting a higher rate of silica gel dissolution at the gel-solution interface might improve the match with the data.

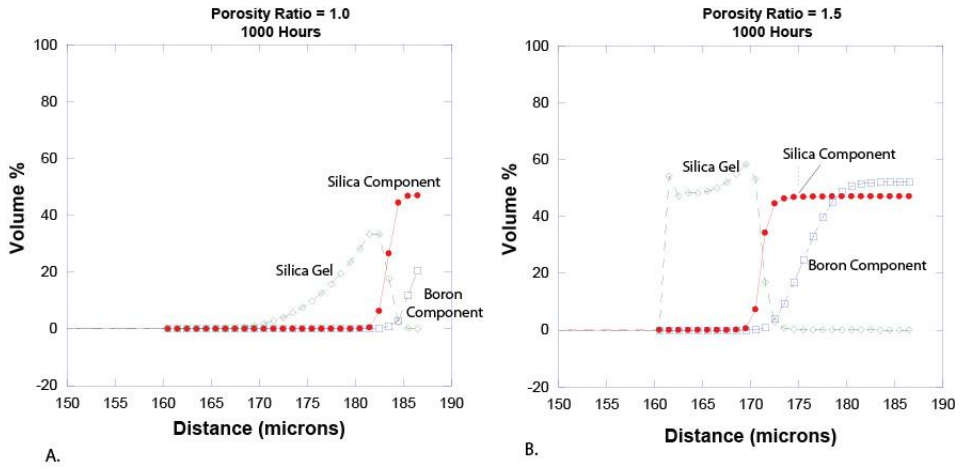

Figure 5-6. Simulations for silica gel formation.

A. Case where recrystallization does not result in densification of the silica gel, and there is no formation of a diffusive PRI-type layer. B. Case where densification results in a PRI-type layer with lower diffusivity, with the result that a diffusion barrier develops.

5.4.2 Single Glass Model

Figure 5-6 illustrates simulation results obtained using a two-component glass. However, similar results can be obtained with congruent dissolution of a single glass composition. In order for reprecipitation of a silica-rich gel layer to occur, the pseudo-solubility of the glass must be higher than the gel solubility. Simply using a TST formulation (Aagaard and Helgeson, 1982) in which the pseudo-solubility (or equilibrium) value for the pristine glass is set at amorphous silica saturation will never result in the formation of a silica gel layer of similar solubility. For the gel layer to form, the solubility of the gel layer must be at least slightly lower. In general, the KμC model predicts that a silica-rich gel layer will form where the solution composition adjacent to the corroding glass is at or close to equilibrium with respect to the gel. Dilute, far from equilibrium conditions in the aqueous phase will generally result in dissolution of the amorphous gel layer, although if the dissolution of this layer is slower than the borosilicate glass dissolution, a silica-rich gel layer may still form. When silica dissolution is sufficiently rapid, no gel layer develops in the case of a dilute solution. Ripening and densification of the silica gel layer, if it occurs more rapidly than the dissolution of the gel, can result in the formation of a diffusion barrier similar to that described in the GRAAL model (Frugier et al., 2008). Formation of a diffusion barrier due to densification will slow both dissolution of the gel layer and corrosion of

the glass, so it is not possible to generate thick gel layers with this mechanism, unless gel densification is significantly delayed. In the case where the gel densifies, the diffusion rate of ions through the gel layer is substantially reduced and the overall rate of corrosion as recorded by the position of the pristine glass front is decreased. Densification here is treated operationally as if the volume of the silica gel layer is greater, which has the effect of reducing the porosity. The densification rate may be rapid, in which case the further corrosion of the borosilicate glass is limited. In the case where the recrystallization and densification rate is slow, the model can represent this as two distinct silica gel phases with differing densities (here represented as differing volumes). If the densification is simply a function of time, then one expects the greatest effect at the water-gel interface (as in the Monte Carlo simulations presented by Cailleteau et al., 2008), since this portion of the gel has existed for the longest period of time. However, other factors may come in to play here and it is possible that the greatest densification will occur immediately adjacent to the pristine glass interface.

5.5 Summary

The essential components of a new kinetic model for borosilicate glass corrosion, which we refer to here as the Kinetic Micro-Continuum or KμC model, are described. The model shares some features with the GRAAL model (Frugier et al, 2008), but is more general in concept and application in that it does not presume *a priori* that the glass corrosion rate is diffusion limited. Instead, diffusion, which is expected to be a function of the evolving porosity and pore structure of the gel layer, is coupled to kinetic dissolution, precipitation, and recrystallization reactions. Corrosion front advance rates may potentially be a function of either the effective diffusivity or the glass reaction kinetics, or both. The latter case, where a mixed diffusion-reaction control occurs, may turn out perhaps to be the most common. The model is able to match effluent chemistry for early times. For later times, the ability of a kinetically-controlled recrystallization model in which gel densification occurs is evaluated in terms of its ability to capture SIMS profiles developed after 1,000 hours of reaction under dilute conditions. The modeling suggests that a densification model is most likely necessary to capture the chemical and evolution of the corrosion products on the glass surface.

6 REFERENCES

Aagaard, P., and H. C. Helgeson (1982), Thermodynamic and kinetic constraints on reaction rates among minerals and aqueous solutions. I. Theoretical considerations, *American Journal of Science*, *282*, 237-285.

Abbas, A., J.-M. Delaye, D. Ghaleb, and G. Calas (2003), Molecular dynamics study of the structure and dynamic behavior at the surface of a silicate glass, *Journal of Non-Crystalline Solids*, *315*, 187-196.

Adiga, S. P., P. Zapol, and L. A. Curtiss (2006), Atomistic simulations of amorphous alumina surfaces, *Physical Review B*, *74*.

Advocat, T., J. L. Crovisier, E. Vernaz, G. Ehret, and H. Charpentier (1991), *HYDROLYSIS OF R7T7 NUCLEAR WASTE GLASS IN DILUTE MEDIA - MECHANISMS AND RATE AS A FUNCTION OF PH*, 57-64 pp.

Beckstein, O., and M. S. P. Sansom (2003), Liquid-vapor oscillations of water in hydrophobic nanopores, *Proceedings of the National Academy of Sciences of the United States of America*, *100*(12), 7063-7068.

Berendsen, H. J. C., J. R. Grigera, and T. P. Straatsma (1987), The missing term in effective pair potentials, *Journal of Physical Chemistry*, *91*, 6269-6271.

Bickmore, B. R., C. J. Tadanier, K. M. Rosso, W. D. Monn, and D. L. Eggett (2004), Bond-Valence methods for pKa prediction: critical reanalysis and a new approach, *Geochim. Cosmochim. Acta*, *68*, 2025-2042.

Blonski, S., and S. H. Garofalini (1993), Molecular dynamics simulations of a-alumina and g-alumina surfaces, *Surface Science*, *295*, 263-274.

Bourg, I. C., and G. Sposito (2010), Connecting the Molecular Scale to the Continuum Scale for Diffusion Processes in Smectite-Rich Porous Media, *Environmental Science & Technology*, *44*(6), 2085-2091.

Bourg, I. C., and G. Sposito (2011), Molecular dynamics simulations of the electrical double layer on smectite surfaces contacting concentrated mixed electrolyte (NaCl-CaCl(2)) solutions, *journal of Colloid and Interface Science*, *360*(2), 701-715.

Bourg, I. C., G. Sposito, and A. C. M. Bourg (2007), Modeling the acid-base surface chemistry of montmorillonite, *Journal of Colloid and Interface Science*.

Brady, P. V., and S. A. Carroll (1994), DIRECT EFFECTS OF CO2 AND TEMPERATURE ON SILICATE WEATHERING - POSSIBLE IMPLICATIONS FOR CLIMATE CONTROL, *Geochim. Cosmochim. Acta*, *58*(7), 1853-1856.

Bryan, C. R., K. B. Helean, B. D. Marshall, and P. V. Brady (2009), Feldspar dissolution rates in the Topopah Spring Tuff, Yucca Mountain, Nevada, *Applied Geochemistry, 24*(11), 2133-2143.

Cailleteau, C., F. Angeli, F. Devreux, S. Gin, J. Jestin, P. Jollivet, and O. Spalla (2008), Insight into silicate-glass corrosion mechanisms, *Nature Materials, 7*, 978-983.

Cailleteau, C., C. Weigel, A. Ledieu, P. Barboux, and F. Devreux (2008), On the effect of glass composition in the dissolution of glasses by water, *Journal of Non-Crystalline Solids, 354*, 117-123.

Cailleteau, C., F. Devreux, O. Spalla, F. Angeli, and S. Gin (2011), Why Do Certain Glasses with a High Dissolution Rate Undergo a Low Degree of Corrosion?, *J. Phys. Chem. C, 115*(13), 5846-5855.

Casey, W. H., H. R. Westrich, J. F. Banfield, G. Ferruzzi, and G. W. Arnold (1993), Leaching and reconstruction at the surfaces of dissolving chain-silicate minerals, *Nature, 366*, 253-256.

Castrillon, S. R.-V., N. Giovambattista, I. A. Aksay, and P. G. Debenedetti (2009), Effect of Surface Polarity on the Structure and Dynamics of Water in Nanoscale Confinement, *Journal of Physical Chemistry B, 113*(5), 1438-1446.

Castrillon, S. R.-V., N. Giovambattista, I. A. Aksay, and P. G. Debenedetti (2009), Evolution from Surface-Influenced to Bulk-Like Dynamics in Nanoscopically Confined Water, *Journal of Physical Chemistry B, 113*(23), 7973-7976.

Chave, T., P. Frugier, A. Ayral, and S. Gin (2007), Solid state diffusion during nuclear glass residual alteration in solution, *Journal of Nuclear Materials, 362*(2-3), 466-473.

Cormier, L., D. Ghaleb, D. R. Neuville, J.-M. Delaye, and G. Calas (2003), Chemical dependence on networktopolgy of calcium aluminosilicate glasses: a computer simulation study, *332*, 255-270.

Criscenti, L. J., J. D. Kubicki, and S. L. Brantley (2006), Silicate glass and mineral dissolution: Calculated reaction paths and activation energies for hydrolysis of a Q3 Si by H3O+ using ab initio methods, *journal of Physical Chemistry A, 110*, 198-206.

Cruz-Chu, E. R., A. Aksimentiev, and K. Schulten (2006), Water-silica force field for simulating nanodevices, *Journal of Physical Chemistry B, 110*(43), 21497-21508.

Cruz-Chu, E. R., A. Aksimentiev, and K. Schulten (2009), Ionic Current Rectification through Silica Nanopores, *J. Phys. Chem. C, 113*(5), 1850-1862.

Cruz-Chu, E. R., T. Ritz, Z. S. Siwy, and K. Schulten (2009), Molecular control of ionic conduction in polymer nanopores, *Faraday Discussions, 143*, 47-62.

Cygan, R. T., J.-J. Liang, and A. G. Kalinichev (2004), Molecular Models of Hydroxide, Oxyhydroxide, and Clay Phases and the Development of a General Forcefield, *Journal of Physical Chemistry B*, *108*, 1255-1266.

Daval, D., I. Martinez, J. Corvisier, N. Findling, B. Goffe, and F. Guyot (2009), Carbonation of Ca-bearing silicates, the case of wollastonite: Experimental investigations and kinetic modeling, *Chemical Geology*, *265*(1-2), 63-78.

Daval, D., I. Martinez, J.-M. Guigner, R. Hellmann, J. Corvisier, N. Findling, C. Dominici, B. Goffe, and F. Guyot (2009), Mechanism of wollastonite carbonation deduced from micro- to nanometer length scale observations, *American Mineralogist*, *94*(11-12), 1707-1726.

Delaye, J.-M., and D. Ghaleb (1996), Molecular dynamics simulation of a nuclear waste glass matrix, *Materials Science and Engineering B37*, 232-236.

Doremus, R. H. (1975), INTERDIFFUSION OF HYDROGEN AND ALKALI IONS IN A GLASS SURFACE, *Journal of Non-Crystalline Solids*, *19*(DEC), 137-144.

Delaye, J.-M., and D. Ghaleb (1996), Molecular dynamics simulation of a nuclear waste glass matrix, *Materials Science and Engineering B37*, 232-236.

Della Valle, R. G., and H. C. Andersen (1992), Molecular dynamics simulation of silica liquid and glass, *Journal of Chemical Physics*, *97*, 2682-2689.

Dove, P. M., and C. M. Craven (2005), Surface charge density on silica in alkali and alkaline earth chloride electrolyte solutions, *Geochemica et Cosmochimica Acta*, *69*, 4963-4970.

Dove, P. M., N. Han, and J. J. De Yoreo (2005), Mechanisms of classical crystal growth theory explain quartz and silicate dissolution behavior, *PNAS*.

Du, J., and A. N. Cormack (2004), The medium range structure of sodium silicate glasses: a molecular dynamics simulation, *Journal of Non-Crystalline Solids*, *349*, 66-79.

Du, J., and A. N. Cormack (2005), Molecular Dynamics Simulations of the Structure and Hydroxylation of Silica Glass Surfaces, *Journal of American Ceramic Society*, *88*, 2532-2539.

Dykhuizen, R. C., and W. H. Casey (1989), AN ANALYSIS OF SOLUTE DIFFUSION IN ROCKS, *Geochim. Cosmochim. Acta*, *53*(11), 2797-2805.

Fenter, P., L. Cheng, C. Park, Z. Zhang, and N. C. Sturchio (2003), Structure of the orthoclase (001)- and (010)-water interfaces by high-resolution X-ray reflectivity, *Geochim. Cosmochim. Acta*, *67*, 4267-4275.

Fenter, P., C. Park, L. Cheng, Z. Zhang, M. P. S. Krekeler, and N. C. Sturchio (2003), Orthoclase dissolution kinetics probed by in situ X-ray reflectivity: Effects of temperature, pH, and crystal orientation, *Geochim. Cosmochim. Acta*, *67*, 197-211.

Ferrand, K., A. Abdelouas, and B. Grambow (2006), Water diffusion in the simulated French nuclear waste glass SON 68 contacting silica rich solutions: Experimental and modeling, *Journal of Nuclear Materials*, *355*(1-3), 54-67.

Feuston, B. P., and S. H. Garofalini (1990), Water-induced relaxation of the vitreous silica surface, *Journal of Applied Physics*, *68*, 4830-4836.

Frizon, F., S. Gin, and C. Jegou (2009), Mass transfer phenomena in nuclear waste packages, *Advances in Transport Phenomena*, *1*, 31-133.

Frugier, P., et al. (2008), SON68 nuclear glass dissolution kinetics: Current state of knowledge and basis of the new GRAAL model, *Journal of Nuclear Materials*, *380*, 8-21.

Garofalini, S. H. (1990), Molecular dynamics computer simulations of silica surface structure and adsorption of water molecules, *Journal of Non-Crystalline Solids*, *120*, 1-12.

Garofalini, S. H. (2001), Molecular Dynamics Simulations of Silicate Glasses and Glass Surfaces, in *Molecular Modelling Theory: Applications in the Geosciences*, edited by R. T. Cygan and J. D. Kubicki, pp. 131-168, Geochemical Society and Mineralogical Society of America, Washington, D. C.

Geneste, G., F. Bouyer, and S. Gin (2006), Hydrogen-sodium interdiffusion in borosilicate glasses investigated from first principles, *Journal of Non-Crystalline Solids*, *352*, 3147-3152.

Gibbs, G. V. (1982) Molecules as models for bonding in silicates, *American Mineralogist*, *67*, 421-450.

Grambow, B. (2006), Nuclear waste glasses - How durable?, *Elements*, *2*(6), 357-364.

Grambow, B. and R. Muller (2001) First order dissolution rate law and the role of surface layers in glass performance assessment, *Journal of Nuclear Materials*, *298*, 112-124.

Guittonneau, C., S. Gin, N. Godon, J. P. Mestre, O. Dugne, and P. Allegri (2011) A 25-year laboratory experiment on French SON68 nuclear glass leached in a granitic environment - First investigations, *Journal of Nuclear Materials*, *408*, 73-89.

Hamilton, J. P., S. L. Brantley, C. G. Pantano, L. J. Criscenti, and J. D. Kubicki (2001), Dissolution of nepheline, jadeite and albite glasses: Toward better models for aluminosilicate dissolution, *Geochimica et Cosmochimica Acta*, *65*, 3683-3702.

Hellmann, R., J.-M. Penisson, R. L. Hervig, J.-H. Thomassin, and M.-F. Abrioux (2003), An EFTEM/HRTEM high-resolution study of the near surface of labradorite feldspar altered at acid pH: evidence for interfacial dissolution-precipitation, *Physics and Chemistry of Minerals*, *30*, 192-197.

Hiemstra, T., and W. H. van Riemsdijk (1996), A Surface Structural Approach to Ion Adsorption: The Charge Distribution (CD) Model, *Journal of Colloid and Interface Science*, *179*, 488-508.

Hiemstra, T., P. Venema, and W. H. van Riemsdijk (1996), Intrinsic Proton Affinity of Reactive Surface Groups of Metal (Hydr)oxides: The Bond Valence Principle, *Journal of Colloid and Interface Science*, *184*, 680-692.

Hochella, M. J. J., and A. F. White (1990), Mineral-Water Interface Geochemistry: An Overview, in *MIneral-Water Interface Geochemistry*, edited by M. F. J. Hochella and A. F. White, pp. 1-16, Mineralogical Society of America, Washington, D.C.

Hochella, M. F. J., S. K. Lower, P. A. Maurice, R. L. Penn, N. Sahai, D. L. Sparks, and B. S. Twining (2008), Nanominerals, Mineral Nanoparticles, and Earth Systems, *Science*, *319*, 1631-1635.

Humphrey, W., A. Dalke, and K. Schulten (1996), VMD: Visual molecular dynamics, *Journal of Molecular Graphics*, *14*(1), 33-&.

Hura, G., D. Russo, R. M. Glaeser, T. Head-Gordon, M. Krack, and M. Parrinello (2003), Water structure as a function of temperature from X-ray scattering experiments and ab initio molecular dynamics, *Physical Chemistry Chemical Physics*, *5*(10), 1981-1991.

Icenhower, J. P., B. P. McGrail, W. J. Shaw, E. M. Pierce, P. Nachimuthu, D. K. Shuh, E. A. Rodriguez, and J. L. Steele (2008), Experimentally determined dissolution kinetics of Na-rich borosilicate glass at far from equilibrium conditions: Implications for Transition State Theory, *Geochim. Cosmochim. Acta*, *72*(12), 2767-2788.

Joseph, S., and N. R. Aluru (2006), Hierarchical multiscale simulation of electrokinetic transport in silica nanochannels at the point of zero charge, *Langmuir*, *22*(21), 9041-9051.

Kerisit, S., and C. X. Liu (2009), Molecular Simulations of Water and Ion Diffusion in Nanosized Mineral Fractures, *Environmental Science & Technology*, *43*(3), 777-782.

Lasaga, A. C. (1998) Kinetic Theory in the Earth Sciences, Princeton University Press, 728pp.

Lasaga, A. C., and A. Luttge (2001), Variation of crystal dissolution rate based on a dissolution stepwave model, *Science*, *291*, 2400-2404.

Lasaga, A. C., J. M. Soer, J. Ganor, T. E. Burch, and K. L. Nagy (1994), Chemical weathering rate laws and global geochemical cycles, *1994*, *58*, 2361-2386.

Leed, E. A., and C. G. Pantano (2003), Computer modeling of water adsorption on silica and silicate glass fracture surfaces, *Journal of Non-Crystalline Solids*, *325*, 48-60.

Leung, K., S. B. Rempe, and C. D. Lorenz (2006), Salt permeation and exclusion in hydroxylated and functionalized silica pores, *Physical Review Letters*, *96*.

Litton, D. A., and S. H. Garofalini (2001), Modeling of hydrophilic wafer bonding by molecular dynamics simulations, *Journal of Applied Physics*, *89*, 6013-6023.

Lynden-Bell, R. M., and J. C. Rasaiah (1996), Mobility and solvation of ions in channels, *Journal of Chemical Physics*, *105*(20), 9266-9280.

Maher, K., C. I. Steefel, D. J. DePaolo, and B. E. Viani (2006), The mineral dissolution rate conundrum: Insights from reactive transport modeling of U isotopes and pore fluid chemistry in marine sediments, *Geochim. Cosmochim. Acta*, *70*(2), 337-363.

Mahadevan, T. S., and S. H. Garofalini (2007), Dissociative water potential for molecular dynamics simulations, *Journal of Physical Chemistry B*, *111*, 8919-8927.

Mahadevan, T. S., and S. H. Garofalini (2008), Dissociative chemisorption of water onto silica surfaces and formation of hydronium ions, *Journal of Physical Chemistry C*, *112*, 1507-1515.

McGrail, B. P., D. H. Bacon, J. P. Icenhower, F. M. Mann, R. J. Puigh, H. T. Schaef, and S. V. Mattigod (2001), Near-field performance assessment for a low-activity waste glass disposal system: laboratory testing to modeling results, *Journal of Nuclear Materials*, *298*, 95-111.

Mellott, N. P. (2003), Multicomonent Aluminosilicate Glasses: Structure and Acid Corrosion, Dissertation thesis, 180 pp, The Pennsylvania State University University Park, PA.

Mills, R. (1973), GENERAL FORMULATION OF N-SITE COHERENT-POTENTIAL APPROXIMATION FOR A DISORDERED MEDIUM, *Physical Review B*, *8*(8), 3650-3660.

Morrow, C. P., S. Nangia, and B. J. Garrison (2009), Ab initio investigation of dissolution mechanisms in aluminosilicate minerals, *Journal of Physical Chemistry A*, *113*, 1343-1352.

Nangia, S., and B. J. Garrison (2009), Ab initio study of dissolution and precipitation reactions from the edge, kink, and terrace sites of quartz as a function of pH, *Molecular Physics*, *107*, 831-843.

Nangia, S. and B. J. Garrison (2009), Advanced Monte Carlo Approach to study evolution of quartz surface during the dissolution process, *Journal of American Chemical Society, 113,* 9538-9546.

Oelkers, E. H. (2001), General kinetic description of multioxide silicate mineral and glass dissolution, *Geochim. Cosmochim. Acta*, *65*, 3703-3719.

Oelkers, E. H., J. Schott, and J. L. Devidal (1994), The effect of aluminum, pH, and chemical affinity on the rates of aluminosilicate dissolution reactions, *Geochim. Cosmochim. Acta*, *58*, 2011-2024.

Ohno, H., S. Kohara, N. Umesaki, and K. Suzuya (2001), High-energy X-ray diffraction studies of non-crystalline materials, *Journal of Non-Crystalline Solids*, *293-295*, 125-135.

Okuno, M., and K. Kawamura (1995), Molecular dynamics calculations for Mg3Al2Si3O12 (pyrope) and Ca3Al2Si3O12 (grossular) glass structures, *Journal of Non-Crystalline Solids*, *191*, 249-259.

Pedone, A., G. Malavasi, M. C. Menziani, A. N. Cormack, and U. Segre (2006), A new self-consistent empirical interatomic potential model for oxides, silicates, and silica-based glasses, *Journal of Physical Chemistry B*, *110*, 11780-11795.

Pelmenschikov, A., H. Strandh, L. G. M. Pettersson, and J. Leszcyzynski (2000), Lattice Resistance to Hydrolysis of Si-O-Si Bonds of Silicate Minerals: Ab Initio Calculations of a Single Water Attack onto the (001) and (111) ß-Cristobalite Surfaces, *Journal of Physical Chemistry B*, 5779-5783.

Pierce, E. M., L. R. Reed, W. J. Shaw, B. P. McGrail, J. P. Icenhower, C. F. Windisch, E. A. Cordova, and J. Broady (2010), Experimental determination of the effect of the ratio of B/Al on glass dissolution along the nepheline ($NaAlSiO_4$)-malinkoite ($NaBSiO_4$) join *Geochimica et Cosmochimica Acta*, *74*, 2634-2654.

Plimpton, S. (1995), Fast Parallel Algorithms For Short-Range Molecular-Dynamics, *Journal of Computational Physics*, *117*, 1-19.

Prakash, S., A. Piruska, E. N. Gatimu, P. W. Bohn, J. V. Sweedler, and M. A. Shannon (2008), Nanofluidics: Systems and applications, *Ieee Sensors Journal*, *8*(5-6), 441-450.

Rana, M. A., and R. W. Douglas (1961), The reaction between glass and water. Part 2. Discussion of the results, *Physics and Chemistry of Glasses*, *2*, 196-205.

Rana, M. A., and R. W. Douglas (1961), The reaction between glass and water. Part I. Experimental methods and observations, *Physics and Chemistry of Glasses*, *2*, 179-195.

Renkin, E. M. (1954), FILTRATION, DIFFUSION, AND MOLECULAR SIEVING THROUGH POROUS CELLULOSE MEMBRANES, *Journal of General Physiology*, *38*(2), 225-243.

Ricci, M. A., F. Bruni, P. Gallo, M. Rovere, and A. K. Soper (2000), Water in confined geometries: experiments and simulations, *Journal of Physics-Condensed Matter*, *12*(8A), A345-A350.

Rotenberg, B., V. Marry, J.-F. Dufreche, E. Giffaut, and P. Turq (2007), A multiscale approach to ion diffusion in clays: Building a two-state diffusion-reaction scheme from microscopic dynamics, *journal of Colloid and Interface Science*, *309*(2), 289-295.

Rotenberg, B., V. Marry, J.-F. Dufreche, N. Malikova, E. Giffaut, and P. Turq (2007), Modelling water and ion diffusion in clays: A multiscale approach, *Comptes Rendus Chimie*, *10*(10-11), 1108-1116.

Rotenberg, B., V. Marry, R. Vuilleumier, N. Malikova, C. Simon, and P. Turq (2007), Water and ions in clays: Unraveling the interlayer/micropore exchange using molecular dynamics, *Geochim. Cosmochim. Acta*, *71*(21), 5089-5101.

Schlegel, M. L., K. L. Nagy, P. Fenter, and N. C. Sturchio (2002), Structures of quartz (10bar10) and (10bar11)-water interfaces determined by X-ray reflectivity and atomic force microscopy of natural growth surfaces, *Geochim. Cosmochim. Acta*, *66*, 3037-3054.

Schoch, R. B., J. Han, and P. Renaud (2008), Transport phenomena in nanofluidics, *Reviews of Modern Physics*, *80*(3), 839-883.

Schweda, P. (1989), Kinetics of alkali feldspar dissolution at low temperature, in *Water-Rock Interaction*, edited by Miles, pp. 609-612, Rotterdam.

Skelton, A. A., P. Fenter, J. D. Kubicki, D. J. Wesolowski, and P. T. Cummings (2011), Simulations of the Quartz(10(1)over-bar1)/Water Interface: A Comparison of Classical Force Fields, Ab Initio Molecular Dynamics, and X-ray Reflectivity Experiments, *J. Phys. Chem. C*, *115*(5), 2076-2088.

Smith, D. E., and L. X. Dang (1994), Computer simulations of NaCl association in polarizable water, *Journal of Chemical Physics*, *100*, 3757-3766.

Smith, W. and Forester, T. R. (1996), DL_POLY_2.0: A general-purpose molecular dynamics simulation package, Journal of Molecular Graphics, 14, 136-141.

Sonnefeld, J. (2001), On the influence of background electrolyte concentration on the position of the isoelectric point and the point of zero charge, *Colloids and Surfaces a-Physicochemical and Engineering Aspects*, *190*(1-2), 179-183.

Sonnefeld, J., M. Lobbus, and W. Vogelsberger (2001), Determination of electric double layer parameters for spherical silica particles under application of the triple layer model using surface charge density data and results of electrokinetic sonic amplitude measurements, *Colloids and Surfaces a-Physicochemical and Engineering Aspects*, *195*(1-3), 215-225.

Stillings, L. L., and S. L. Brantley (1995), Feldspar dissolution at 25oC and pH 3: Reaction stoichiometry and the effect of cations, *Geochim. Cosmochim. Acta*, *59*, 1483-1496.

Stillings, L. L., S. L. Brantley, and M. L. Machesky (1995), Proton adsorption at an adularia feldspar surface, *Geochim. Cosmochim. Acta*, *59*, 1473-1482.

Soules, T. F. (1979), A molecular dynamic calculation of the structure of sodium silicate glasses, *Journal of Chemical Physics*, *71*, 4570-4578.

Toney, M. F., J. N. Howard, J. Richer, G. L. Borges, J. G. Gordon, O. R. Melroy, D. G. Wiesler, D. Yee, and L. B. Sorensen (1995), DISTRIBUTION OF WATER-MOLECULES AT AG(111)/ELECTROLYTE INTERFACE AS STUDIED WITH SURFACE X-RAY-SCATTERING, *Surface Science*, *335*(1-3), 326-332.

Tournie, A., P. Ricciardi, and P. Colomban (2008), Glass corrosion mechanisms: A multiscale analysis, *Solid State Ionics*, *179*(38), 2142-2154.

Tsomaia, N., S. L. Brantley, J. P. Hamilton, C. G. Pantano, and K. T. Mueller (2003), NMR evidence for formation of ocathedral and tetrahedral Al and repolymerization of the Si network during dissolution of aluminosilicate glass and crystal, *American Mineralogist*, *88*, xxx-xxx.

Van Beest, B. W. H., G. J. Kramer, and R. A. van Santen (1990), Force Fields for Silicas and Aluminophosphates Based on Ab Initio Calculations, *Physical Review Letters*, *64*, 1955-1958.

Van Iseghem, P., K. Lemmens, E. Valcke, and M. Aertsens (2009), SCK center dot CEN R&D ON THE INTERACTION BETWEEN NUCLEAR WASTE GLASS AND CLAY NEAR- AND FAR-FIELD MATERIALS, in *Environmental Issues and Waste Management Technologies in the Materials and Nuclear Industries Xii*, edited by A. O. T. Cozzi, pp. 103-114.

Van Iseghem, P., M. Aertsens, S. Gin, D. Deneele, B. Grambow, D. Strachan, P. McGrail, and G. Wicks (2009), GLAMOR - OR HOW WE ACHIEVED A COMMON UNDERSTANDING ON THE DECREASE OF GLASS DISSOLUTION KINETICS, in *Environmental Issues and Waste Management Technologies in the Materials and Nuclear Industries Xii*, edited by A. O. T. Cozzi, pp. 115-126.

Verhoef, A. H., and H. W. den Hartog (1995), Structure and dynamics of alkali borate glasses: a molecular dynamics study, *Journal of Non-Crystalline Solids*, *182*, 235-247.

Verney-Carron, A., S. Gin, and G. Libourel (2008), A fractured roman glass block altered for 1800 years in seawater: Analogy with nuclear waste glass in a deep geological repository, *Geochim. Cosmochim. Acta*, *72*, 5372-5385.

Verney-Carron, A., S. Gin, P. Frugier, and G. Libourel (2010), Long-term modeling of alteration-transport coupling: Application to a fractured Roman glass, *Geochim. Cosmochim. Acta*, *74*(8), 2291-2315.

Wallmann, K. (2001), Controls on the Cretaceous and Cenozoic evolution of seawater composition, atmospheric CO2 and climate, *Geochim. Cosmochim. Acta*, *65*(18), 3005-3025.

Wang, Y., C. Bryan, and H. Xu (2003), Nanogeochemistry: Geochemical reactions and mass transfers in nanopores, *Geology*, *31*, 387-390.

Washton, N. M., S. L. Brantley, and K. T. Mueller (2008), Probing the molecular-level control of aluminosilicate dissolution: A sensitive solid-state NMR proxy for reactive surface area, *Geochimica et Cosmochimica Acta*, *72*, 5949-5961.

Wasserman, E., B. Wood, and J. Brodholt (1995), THE STATIC DIELECTRIC-CONSTANT OF WATER AT PRESSURES UP TO 20 KBAR AND TEMPERATURES TO 1273-K - EXPERIMENT, SIMULATIONS, AND EMPIRICAL EQUATIONS, *Geochim. Cosmochim. Acta*, *59*(1), 1-6.

Wasserman, E., B. Wood, and A. Davies (1995), EQUATION OF STATE FOR AQUEOUS SILICA SPECIES AT PRESSURES FROM 1 BAR TO 20 KBAR AND TEMPERATURES FROM 25-DEGREES TO 900-DEGREES-C BASED ON SIMULATED VALUES OF THE DIELECTRIC-CONSTANT, *Chemical Geology*, *121*(1-4), 3-9.

White, A. F., and S. L. Brantley (2003), The effect of time on the weathering of silicate minerals: why do weathering rates differ in the laboratory and the field?, *Chemical Geology*, *202*, 479-506.

Zhang, L. and A. Luttge (2009) Theoretical approach to evaluating plagioclase dissolution mechanisms, *Geochimica et Cosmochimica Acta, 73,* 2832-2849.

Zhmud, B. V., W. A. House, and F. H. Denison (1997), Release kinetics and concentration profile of dissolved silicon in compacted sediments, *Journal of the Chemical Society-Faraday Transactions*, *93*(19), 3473-3478.

Zhmud, B. V., J. Sonnefeld, and W. A. House (1997), Role of ion hydration in the charge regulation at the surface of porous silica gel, *Journal of the Chemical Society-Faraday Transactions*, *93*(17), 3129-3136.

ELECTRONIC DISTRIBUTION

EXTERNAL

Bacon, Diana, Diana.bacon@pnl.gov
Pacific Northwest National Laboratory
P.O. Box 999
Richland, WA 99352

Bourg, Ian, icbourg@lbl.gov
Earth Sciences Division
Lawrence Berkeley National Laboratories
Berkeley, California 94701

Icenhower, Johnathan, jonathan.icenhower@gmail.com
Earth Sciences Division
Lawrence Berkeley National Laboratories
Berkeley, California 94701

Mueller, Karl, karl.mueller@pnl.gov
Pacific Northwest National Laboratory
P.O. Box 999
Richland, WA 99352

Pierce, Eric, pierceem@ornl.gov
Oak Ridge National Laboratories
P.O. Box 2008
Oak Ridge, TN 37831

Ryan, Joseph, joe.ryan@pnl.gov
Pacific Northwest National Laboratory
P.O. Box 999
Richland, WA 99352

Steefel, Carl, CISteefel@lbl.gov
Earth Sciences Division
Lawrence Berkeley National Laboratories
Berkeley, California 94701

Strachan, Denis, denis.stachan@pnl.gov
Pacific Northwest National Laboratory
P.O. Box 999
Richland, WA 99352

Vienna, John, john.vienna@pnl.gov
Pacific Northwest National Laboratory
P.O. Box 999
Richland, WA 99352

Zapol, Peter, Zapol@anl.gov
Materials Science Division
Argonne National Laboratory
9700 S. Cass Avenue
Argonne, IL 60439.

INTERNAL

Aidun, John	MS 1322	Advanced Device Technologies
Brady, Patrick	MS 0754	Geoscience Research and Applications
Cygan, Randall	MS 0754	Geochemistry
Edwards, Carter	MS 1318	Multiphysics Simulation Technologies
Freeze, Goeff	MS 1370	Nuclear Fuel Cycle Systems Engineering and Integration
Jove-Colon, Carlos	MS 0779	Radiological Consequence Management and Responsibility
Rigali, Mark	MS 0754	Geochemistry
Sassani, David	MS 0736	Advanced Systems Analysis
Schultz, Peter	MS 1322	Advanced Device Technologies
Summers, Randall	MS 1321	Multiphysics Simulation Technologies
Zeitler, Todd	MS 0754	Geochemistry

1 MS0899 RIMS-Reports Management, 9532


Sandia National Laboratories